THE GEOLOGICAL SOCIETY OF AMERICA®

Exhuming a cold case: The early granodiorites of the northwest Iberian Variscan belt—A Visean magmatic flare-up?

G. Gutiérrez-Alonso[1,2], J. Fernández-Suárez[3], Alicia López-Carmona[1,2], and Andreas Gärtner[4]

[1]DEPARTAMENTO DE GEOLOGÍA, UNIVERSITY OF SALAMANCA, PLAZA DE LOS CAÍDOS S/N, 37008 SALAMANCA, SPAIN
[2]GEOLOGY AND GEOGRAPHY DEPARTMENT, TOMSK STATE UNIVERSITY, LENIN STREET 36, TOMSK 634050, RUSSIA
[3]DEPARTAMENTO DE PETROLOGÍA Y GEOQUÍMICA, UNIVERSIDAD COMPLUTENSE AND IGEO, CSIC (INSTITUTO DE GEOCIENCIAS, CENTRO MIXTO DEL CONSEJO SUPERIOR DE INVESTIGACIONES CIENTÍFICAS), 28040 MADRID, SPAIN
[4]MUSEUM FÜR MINERALOGIE UND GEOLOGIE, SEKTION GEOCHRONOLOGIE, GEOPLASMA LAB, SENCKENBERG NATURHISTORISCHE SAMMLUNGEN DRESDEN, KÖNIGSBRÜCKER LANDSTRASSE 159, 01109 DRESDEN, GERMANY

ABSTRACT

In this study we report laser ablation–inductively coupled plasma–mass spectrometer U-Pb ages of granitoids from the so-called early granodiorites of the northwest Iberian Variscan belt. The U-Pb results attest to significant magmatic activity in Visean time (ca. 347–337 Ma) that generated a hitherto poorly constrained granitoid suite in the northwest Iberian tract of the western European Variscan belt realm. This early Carboniferous suite (ECS) is mainly composed of peraluminous cold and hot crustal granodiorites and monzogranites with minor associated mafic rocks that attest to minor involvement of mantle melting. Based on the geochronological and geochemical data, we compare the Visean granitoids with younger Variscan granitoids in northwest Iberia and, in view of the tectonothermal scenarios of the Variscan collision in northwest Iberia, propose a model for the genesis of the ECS in northwest Iberia that involves rapid melting upon fast exhumation of the thickened Gondwanan crust in the course of the protracted Variscan collision.

LITHOSPHERE; v. 10; no. 2; p. 194–216 | Published online 9 February 2018 https://doi.org/10.1130/L706.1

INTRODUCTION

Variscan granitoid magmatism in northwest Iberia is an example of the intimate link between granitoid magma production and plate convergence–collisional–postcollisional geodynamic scenarios. In the western European Variscan belt realm (WEVB, Fig. 1), the major stages of convergent tectonics and their aftermath are recorded by granitoid suites generated in a time span of ~50 m.y. (ca. 340–290 Ma). There is, however, some controversy regarding (1) whether there was a significant magmatic event in the early Carboniferous, for which there was previously scarce evidence (see following), and (2) whether the Variscan magmatic activity was continuous or occurred through discrete and relatively short-lived pulses. Unravelling these issues is one of the key elements to better constrain and interpret the different processes involved in the collisional scenarios that led to the Variscan orogeny in Iberia during late Paleozoic time (e.g., Matte, 2001; Martínez Catalán et al., 2007; Ballèvre et al., 2009; Arenas et al., 2016; Díez Fernández et al., 2016) and the subsequent development of the Ibero-Armorican arc (e.g., Weil et al., 2013, and references therein; Fig. 1).

The hypotheses that support rather continuous magmatic activity are mainly derived from the combined interpretation of radiometric ages of granitoids obtained by different methods (U-Pb, Rb-Sr, ^{40}Ar-^{39}Ar, K-Ar; e.g., Serrano Pinto et al., 1987; Díaz Alvarado et al., 2013; Martínez Catalán et al., 2014) and the numerical modeling of the thermal evolution of the orogen, including radioactive heat production (e.g., Bea et al., 1999, 2003; Bea, 2012; Alcock et al., 2015). In essence, these hypotheses view melt production in the collisional scenario mainly as the result of severe crustal thickening of a fertile (graywacke and pelite rich) crust followed by an interval of thermal relaxation (e.g., Martínez-Catalán et al., 2014) accompanied by melting of the thickened crust.

The advent of a large amount of more precise U-Pb age data on Variscan granitoids (and some volcanic rocks) from northwest Iberia in recent years (e.g., compilation in Gutiérrez-Alonso et al., 2011; Martínez Catalán et al., 2014) has provided a more focused picture of the magmatic history of the WEVB, providing solid ground for interpretations that link periods of more intense magmatic activity with large-scale crust-mantle processes involved in the collisional orogeny and the subsequent development of the West European Variscan Belt (e.g., Castro et al., 1999, 2000; Fernández-Suárez et al., 2000; Villaseca et al., 2009, 2011; Gutiérrez-Alonso et al., 2011; Orejana et al., 2012; López-Moro et al., 2018).

Based on those more precise U-Pb ages, three main pulses of magmatic activity seem to be well established.

1. The postorogenic granitoid suite (POS) (ca. 305–290 Ma), known classically as G3-G4 or late granites in the regional literature (Capdevila, 1969; Capdevila and Floor, 1970; Galán et al., 1996), intrude all the structural domains of the orogen, including the foreland fold and thrust belt, which makes the WEVB unique (see Gutiérrez-Alonso et al., 2011). The POS includes a large number of volumetrically minor intrusions of mafic and ultramafic rocks (e.g., Franco and García de Figuerola, 1986; Bea et al., 2006a; Villaseca et al., 2011; Orejana et al., 2012, 2015). This magmatic event has been extensively studied and dated (e.g., Ugidos and Recio, 1993;

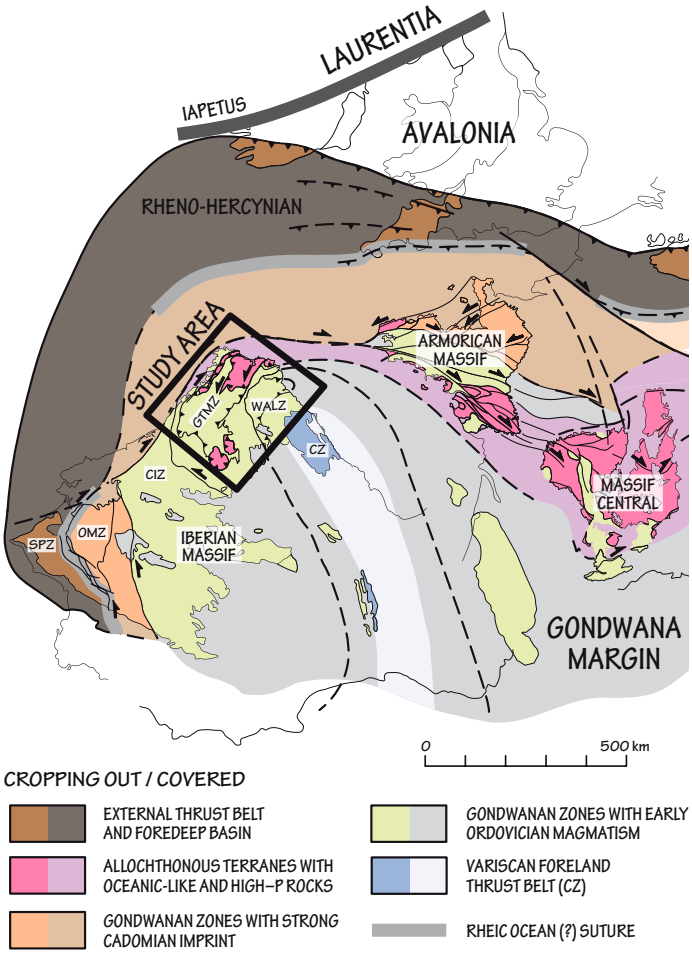

Figure 1. Permian reconstruction of the West European Variscan Belt (according to Ballèvre et al., 2014; modified by Fernández-Lozano et al., 2016). The square indicates the location of the study area (Fig. 2); P—pressure. CZ—Cantabrian zone; WALZ—West Asturian Leonese zone; CIZ—Central Iberian zone, including part of the Galicia-Tras-os-Montes zone (GTMZ); OMZ—Ossa Morena zone; SPZ—South Portuguese zone.

Moreno-Ventas et al., 1995; Bea et al., 1999, 2006a; Castro et al., 1999; Villaseca et al., 1998, 1999; Cuesta and Gallastegui, 2007; Fernández-Suárez et al., 2000, 2011; Orejana et al., 2009; Gutiérrez-Alonso et al., 2011). The POS has been interpreted as generated by lithospheric delamination triggered by the oroclinal bending of the mountain belt (Fernández-Suárez et al., 2000; Gutiérrez-Alonso et al., 2004, 2011, and references therein).

2. Synextensional collapse granitoids (ca. 325–315 Ma), mostly crustal (S-type) peraluminous leucogranites, were generated by decompression melting following the extensional collapse of the mountain belt (e.g., Dias et al., 1998; Fernández-Suárez et al., 2000; Valle Aguado et al., 2005; Teixeira et al., 2012; Díez Fernández and Pereira, 2016; López-Moro et al., 2018; Pereira et al., 2018).

3. A third suite of Variscan granitoids (the object of this study), putatively older than the syntectonic leucogranitoids, was postulated in the early works of Den Tex (1966), Capdevila (1969), and Capdevila et al. (1973), based mainly on the presence of a tectonic foliation and a more mafic composition than that of the synextensional granitoids. They are commonly labeled Granodioritas precoces (early granodiorites), following De Pablo Maciá (1981) and González Lodeiro et al. (1984), and were interpreted as being deeper seated intrusions than the POS. In the following we refer to this suite as the ECS (early Carboniferous suite). Gallastegui (2005) dated the intrusion of Bayo-Vigo applying U-Pb zircon dating, and Gloaguen (2006) and Gloaguen et al. (2006) used U-Th-Pb chemical dating of monazite to date the Chantada intrusion (both belonging to this group; Fig. 2), obtaining moderately precise ages between ca. 350 and 330 Ma. Moreover, there are K-Ar and Rb-Sr isochron ages ca. 340 Ma in granitoids putatively belonging to this suite in northwest Iberia (see compilation in Serrano Pinto et al., 1987). In addition, ca. 340 Ma zircon xenocrysts have been found in the ca. 320 Ma syntectonic leucogranitoids of the Tormes dome and surrounding areas (López-Moro et al., 2018), in the ca. 305 Ma Toledo Anatectic Complex (Martín Garro, 2015), and as detrital zircons in Variscan synorogenic sediments of the Cantabrian zone (Pastor-Galán et al., 2013) and the Central Iberian and Galicia Tras-os-Montes zones (Da Silva et al., 2015; Martínez Catalán et al., 2016). Furthermore, volcanic rocks (ash-fall beds) in the Cantabrian zone have been recently dated as ca. 340 Ma (Merino-Tomé et al., 2017). Monazite and rutile of this age have been found in in migmatitic rocks of the Basal Units of the allochthonous complexes in northwest Iberia (Abati and Dunning, 2002). However, despite the data cited above, the existence of a suite of Variscan granitoids older than ca. 330 Ma has been called into question (e.g., Rodríguez et al., 2007; Martínez Catalán et al., 2014; Alcock et al., 2015).

The main objective of this study is to test the existence of an older (early Carboniferous) suite of Variscan intrusions in northwest Iberia that would broadly correspond to the G1 type of Capdevila et al. (1973) or early granodiorites of De Pablo Maciá (1981). This early Carboniferous suite is widely represented in other areas of the WEVB (e.g., Schaltegger, 1997, 2000; Schulmann et al., 2002; Eichhorn et al., 2000; Cartannaz et al., 2007; Li et al., 2014; Mezger and Gerdes, 2016; Tabaud et al., 2015; Galán et al., 1997; Ledru et al., 2001; Rossi et al., 2009; Kubínová et al., 2017; Laurent et al., 2017; Žák et al., 2017), including the Ossa Morena zone of southwest Iberia (e.g., Dallmeyer et al., 1995; Ordóñez Casado, 1998; Montero et al., 2000; Ordóñez Casado et al., 2008; Romeo et al., 2006; Jesus et al., 2007; Pin et al., 2008; Pereira et al., 2009, 2015; Braid et al., 2012; Dupuis et al., 2014; Gladney et al., 2014; Cambeses et al., 2015). In the Ossa Morena zone rocks belonging to this suite are the volumetrically dominant granitoids, whereas in northwest Iberia the volumetrically dominant granitoids are both the previously described syntectonic leucogranites and the postorogenic granites (Fig. 2).

To perform this test we undertook laser ablation–inductively coupled plasma–mass spectrometer (LA-ICP-MS) U-Pb dating of zircons from 13 samples taken from intrusions ascribed to the early granodiorites (Fig. 2) in northwest Iberia. Thorough reviews of the main geological and petrological features of these granitoids can be found in González Lodeiro et al. (1984), Bellido Mulas et al. (1987), and Gallastegui (2005). As shown here, our work proves beyond reasonable doubt that such a group of older granitoids exists in northwest Iberia. Their ages are constrained between 347 and 337 Ma (Visean), an age bracket similar to that of their west European counterparts (see references in paragraph above).

REGIONAL SETTING

The collision between Laurussia and Gondwana and several putative microplates resulted in the late Paleozoic orogen in central and western Europe known as the Variscan orogen (e.g., Nance et al., 2010), that led to the amalgamation of Pangea. The WEVB is classically divided into a number of zones based on the differences in the early Paleozoic stratigraphy as well as structural style, metamorphism, and magmatism (Lotze, 1945; Julivert, 1971; Franke, 1989; Martínez Catalán et al., 1997, 2007; Ballèvre et al., 2014). These zones broadly correspond to increasing distance from the Gondwanan margin toward the Rheic Ocean (Fig. 1).

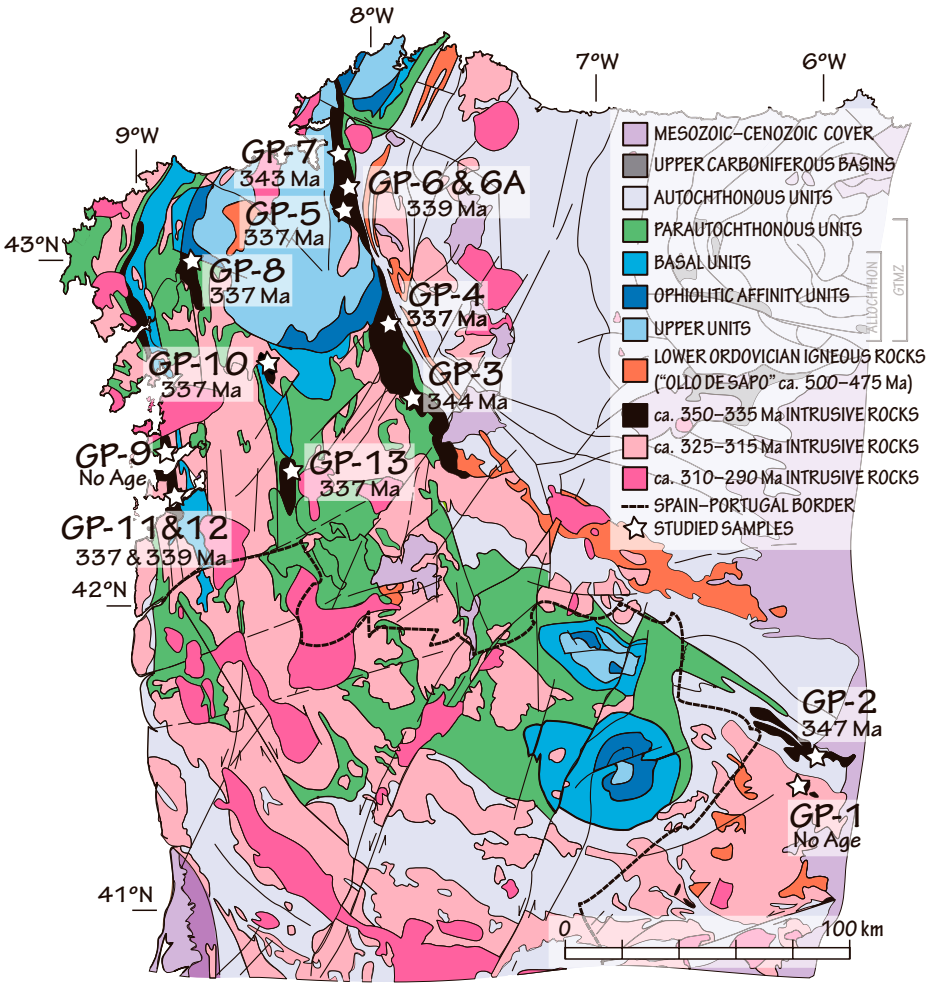

Figure 2. Simplified geological map of northwest Iberia (modified after Rodríguez Fernández et al., 2004; GEODE, 2017) showing the main units and the outcrops of Variscan granitoids as well as the location of the studied samples belonging to the early Carboniferous suite (ECS). GTMZ—Galicia-Tras-os-Montes zone.

The northwest Iberian massif (Fig. 1) includes Neoproterozoic rocks with Gondwanan (North Africa) affinity, which form the basement for late Ediacaran–early Cambrian subduction-related and early Paleozoic passive margin sequences, respectively (e.g., Rodríguez Alonso et al., 2004; Murphy et al., 2008; Fernández-Suárez et al., 2014; Rubio-Ordóñez et al., 2015). In Late Devonian and Carboniferous time, the collision of the passive margin of Gondwana (acting as the lower plate) with Laurussia (upper plate) resulted in the Variscan orogen and ultimately in the amalgamation of Pangea (e.g., Matte, 1986, 2001; Murphy et al., 2009; Kroner and Romer, 2013).

The earliest record of Variscan deformation in Iberia is preserved at ca. 400 Ma in the allochthonous units (Figs. 1 and 2) (e.g., Dallmeyer and Gil Ibarguchi, 1990; Gómez Barreiro et al., 2006); the continent-continent collision occurred later, ca. 365 Ma (e.g., Dallmeyer et al., 1997; López-Carmona et al., 2014), when the Gondwanan, most external, part of the margin (the Basal Units, Fig. 2) attained its maximum depth of burial under the continental units now preserved in the upper units (Fig. 2). Deformation migrated toward the east (in present-day coordinates), culminating with the development of the foreland fold and thrust belt (the Cantabrian zone) during Late Mississippian–Early Pennsylvanian time (ca. 325–320 Ma). After these events, the orogenic edifice was buckled around a vertical axis, giving rise to the orocline known as the Iberian Armorican arc, or the Cantabrian orocline (e.g., Weil et al., 2013; Pastor-Galán et al., 2015, 2016).

A sequence of magmatic events is recorded in the rocks affected by the Variscan orogeny of Iberia. Some of them developed prior to the Variscan orogeny, while others took place coevally, or immediately after, and can be summarized as follows. (1) A subduction-related Cadomian (ca. 600 Ma) magmatic event dominated by I-type granitoids and volcanic rocks (Fernández-Suárez et al., 1998; Rubio-Ordóñez et al., 2015), which is scarcely represented in northwest Iberia. (2) A voluminous extension-related late Cambrian to Early Ordovician magmatic event (ca. 490–470 Ma) is generally interpreted to be linked to the opening of the Rheic Ocean (Valverde-Vaquero and Dunning, 2000; Murphy et al., 2006; Bea et al., 2006b; Montero et al., 2007; Díez Montes et al., 2010; Talavera et al., 2013). (3) A scarcely represented volcanic event ca. 400–390 Ma is interpreted to represent the extension associated with the far-field effect of the Rheic ridge subduction under its northern margin (Gutiérrez-Alonso et al., 2008). (4) Carboniferous synorogenic (Variscan) magmatism was concentrated between ca. 325 and 315 Ma (see Introduction). (5) Postorogenic magmatism peaked ca. 305 and 290 Ma, when voluminous granitoids and some mafic rocks with their extrusive equivalents were emplaced and erupted in both the internal and external zones of the orogen.

MAIN FEATURES OF THE ECS GRANITOIDS

The dated intrusions belonging to the ECS show elongated shapes that follow the structural grain of the area where each of them was emplaced

(Fig. 2). This feature has been classically interpreted as the result of their emplacement having occurred at deeper crustal levels than that of the younger granitoid groups (Capdevila et al., 1973; Bellido Mulas et al., 1987). Figure 2 is a simplified geological map of northwest Iberia showing the plutons dated in this study and the location of each sample.

Here we present a brief description of the samples from this study together with a summary of the main features of the intrusions taken from the literature (González Lodeiro et al., 1984; Bellido Mulas et al., 1987; Barrera et al., 1989; Gallastegui, 2005).

In general, the granitoid rocks belonging to the ECS are mainly porphyritic biotite ± amphibole granodiorites and biotite ± muscovite monzogranites often containing microgranular enclaves (tonalites and quartz-diorites; e.g., Gallastegui, 2005) and less abundant country-rock xenoliths.

The Ricobayo pluton (GP-2) is the southernmost of the studied intrusions. It intruded early Paleozoic sedimentary rocks of the autochthonous sequences of the Central Iberian zone (CIZ). The intrusion is made up mainly of heterogranular biotite and two-mica monzogranites, partially episyenitized (López-Moro et al., 2013), displaying a cataclastic to protomylonitic texture imparted by a late to post-Variscan shear zone (Villalcampo shear zone; González-Clavijo et al., 1993) dated as 306 ± 6 Ma (Gutiérrez-Alonso et al., 2015).

Samples GP-3 and GP-4 are from the Chantada-Taboada composite pluton. The intrusion is essentially composed of biotite monzogranites that intruded metasedimentary rocks of the Galicia-Tras-os-Montes (GTM) parautochthonous unit. The only previous radiometric ages are a K-Ar age (282 Ma; Ries, 1979) and U-Th-Pb chemical monazite date (ca. 350–330 Ma; Gloaguen, 2006; Gloaguen et al., 2006). The northeast part of this intrusion is affected by the subvertical, strike-slip, left-lateral late Variscan Valdoviño fault (Parga-Pondal et al., 1982; Fernández and Llana-Fúnez, 2016) that imparted a strong mylonitic foliation.

The Espenuca intrusion (samples GP-5, GP-6, and GP-7) is an elongated pluton, more than 65 km in length, intruding the GTM parautochthonous unit and the allochthonous complexes (upper unit of the Órdenes complex). It is mainly composed of biotite ± muscovite monzogranites and was strongly affected by the Valdoviño fault in its western part (Ortega et al., 1994). Ortega (1998) obtained an Rb-Sr isochron age of 319 ± 20 Ma for the main facies of this granitoid.

The Santa Comba granodiorite, also known as Negreira granodiorite in the regional literature (Parga Pondal, 1956), is a north-south–elongated body (sample GP-8) intruding the GTM parautochthonous unit. The studied intrusion is affected in its northern boundary by the Pico Sacro detachment, which is the lower limit of the allochthonous units in this area, and interpreted to be of late Carboniferous age (Gómez-Barreiro et al., 2010). This intrusion is locally affected by the Padrón dome migmatites that are interpreted to have formed ca. 320 Ma (Díez Fernández et al., 2017, and references therein).

Sample GP-10 was collected in the Meabia pluton, which is the only one of the studied plutons to have clearly intruded in the allochthonous units (Lalín Forcarey Unit; Klein, 1982; Marquínez, 1984).

The Bayo-Vigo granodiorite is a north-south–elongated intrusion located to the west of the westernmost allochthonous unit (Malpica-Tui Complex) and separated from it through the ca. 307 Ma Malpica-Lamego shear zone (^{40}Ar-^{39}Ar; Rodríguez et al., 2003; Gutiérrez-Alonso et al., 2015). There are minor Mg-K biotite-rich quartz-diorite rocks associated with this intrusion. These mafic rocks are known in the Variscan regional literature as Vaugnerites; because of the widespread use of this term (cf. von Raumer et al., 2014, and references therein) we retain its use herein.

The Bayo-Vigo intrusion was studied in detail by Gallastegui (2005), who obtained a U-Pb age (isotope dilution–thermal ionization mass spectrometry on multigrain zircon fractions) of 349 ± 15 Ma. Two samples from this intrusion were collected for this study: sample GP-11 represents the main granodiorite facies and sample GP-12 represents the spatially associated vaugnerites. Both samples were taken ~1 km apart.

Sample GP-13 was collected in the Avión intrusion, a deformed north-south–elongated granodiorite pluton (Monteserín, 1981; Barrera et al., 1989) that intrudes the parautochthonous units and the southernmost part of the Basal Units cropping out in the Lalín-Forcarey domain (Ordenes Complex).

GENERAL GEOCHEMICAL FEATURES AND CLASSIFICATION OF THE ECS GRANITOIDS

The rocks putatively belonging to the ECS show a considerable variety of mineralogical and geochemical features, and the granitoids are in some cases associated with volumetrically minor mantle-derived mafic rocks, including vaugnerites (see compilation in Gallastegui, 2005).

Although the main aim of this study is to prove the hitherto questioned existence of an early Carboniferous granitoid suite in northwest Iberia, as well as to propose a geodynamic scenario for its genesis, we use whole-rock major and trace element analyses (analysis performed by Actlabs, www.actlabs.com) of the dated rocks (Table 1) along with some geochemical data from Gallastegui (2005) for the Bayo-Vigo granodiorites and vaugnerites, López-Moro et al. (2013) for the Ricobayo granite, and from the Spanish geological survey (IGME, Instituto Geológico y Minero de España) reports for the Chantada-Taboada, Meabia, and Avión intrusions (Barrera et al., 1989) to provide an overview of the main geochemical features of this granitoid suite.

With the exception of the vaugnerites, the granitoid samples have SiO_2 contents ranging between ~68% and 74%, low CaO, MgO, and ASI (molar $Al_2O3/Na_2O + K_2O + CaO$) values between 1.05 and 1.3, and Rb/Sr ratios between ~0.5 and 9.0.

Based on their major element composition and following the nomenclature of Frost et al. (2001), the granitoid rocks of the ECS of Iberia (Table 1; Fig. 3) can be classified as magnesian (with a transition to ferroan in the most silicic terms), alkali-calcic to calc-alkalic and peraluminous (Shand, 1943), with the exception of the more mafic terms, which are metaluminous. Note that in the SiO_2 versus $Na_2O + K_2O$-CaO diagram the more silicic terms shift to more calc-alkalic compositions, as noted by Frost et al. (2001) for the postorogenic Caledonian granites of Britain.

The analyzed samples have moderate rare earth element contents with LaN/LuN values between 7 and 40, and all samples display a negative Europium anomaly with Eu/Eu* values ranging between ~0.3 and 0.8 (Table 1; Fig. 4A).

The normal mid-oceanic ridge basalt (N-MORB) normalized plots (Fig. 4B) show a marked enrichment in the incompatible elements with positive anomalies in K and Pb and negative anomalies in Nb and Ti.

In the trace element discrimination diagrams Rb versus Y + Nb and Y versus Nb (Pearce et al., 1984; Figs. 4C, 4D), the ECS rocks straddle the fields of syncollisional granitoids and that of volcanic arc granites, a feature characteristic of many granitoids that are neither true volcanic arc nor Himalayan type (cf. Hopkinson et al, 2017). The same pattern is displayed by the granitoids of the POS of northwest Iberia on these diagrams (cf. Fernández-Suárez et al., 2000, 2011).

Although the composition of the mafic rocks (vaugnerites) in the Bayo-Vigo intrusion has been plotted in Figures 3 and 4, our focus is on the granitoids. In the context of the objective of this work, the presence of these mafic rocks, that also occur in other intrusions of the ECS (Bellido Mulas et al., 1987; Gallastegui, 2005) but have not been dated, is used as an argument in the discussion to strengthen the notion that the genesis of the ECS was accompanied by some degree of partial mantle melting

TABLE 1. WHOLE-ROCK GEOCHEMISTRY FOR THE U-Pb DATED SAMPLES

Granite unit sample	GP-1	GP-2	GP-3	GP-4	GP-5	GP-6	GP-6A	GP-7	GP-8	GP-9	GP-10	GP-11	GP-12	GP-13
SiO_2	68.7	73.3	67.9	70.9	74.2	70.7	68.0	74.9	73.3	69.9	72.4	67.4	57.0	72.3
Al_2O_3	16.7	15.3	15.5	15.0	14.6	15.2	15.2	13.6	13.9	15.2	13.5	16.3	15.8	13.4
FeO_t	2.3	1.2	3.7	2.7	1.2	2.3	2.2	1.2	2.2	1.7	2.5	3.4	5.7	2.4
MnO	0.0	0.0	0.1	0.0	0.0	0.0	0.0	0.0	0.0	0.0	0.1	0.0	0.1	0.1
MgO	0.8	0.2	1.5	1.0	0.2	0.4	0.6	0.1	0.7	0.5	0.4	1.5	4.4	0.7
CaO	1.4	0.6	2.1	1.5	0.2	0.3	0.8	1.3	1.3	0.4	0.6	2.0	5.8	0.5
Na_2O	3.5	3.4	2.9	2.8	2.1	1.0	2.6	3.3	3.3	1.9	3.3	3.1	2.8	2.9
K2O	5.2	4.4	3.9	4.8	4.5	5.6	6.0	3.5	5.0	6.1	3.8	4.8	3.2	4.1
TiO_2	0.3	0.1	0.6	0.4	0.1	0.3	0.4	0.1	0.2	0.2	0.3	0.5	0.9	0.2
P_2O_5	0.3	0.2	0.3	0.2	0.2	0.2	0.5	0.1	0.2	0.2	0.1	0.3	0.4	0.1
LOI	0.9	0.8	1.2	1.1	2.1	2.4	2.0	0.7	0.6	2.4	1.6	1.2	1.7	1.9
Total	100.5	99.8	100.0	100.7	99.5	98.6	98.5	98.8	101.0	98.6	98.8	101.0	98.4	98.9
ASI	1.19	1.34	1.21	1.20			1.26	1.18	1.05		1.27	1.17	0.85	1.33
*T*zirc (°C)	780	714	837	789			815	681	776		800	811	764	775
Sc	4	2	9	6	8	6	2	3	5	5	4	8	21	5
Be	11	8	4	8	6	5	15	13	11	15	6	5	7	10
V	24	5	57	36	<5	32	23	7	25	15	18	47	148	22
Cr	130	<20	180	50	140	40	130	30	150	30	170	60	250	50
Co	4	1	9	6	1	4	3	1	4	6	3	8	20	4
Ni	<20	<20	20	<20	<20	<20	<20	<20	<20	<20	<20	<20	30	<20
Cu	<10	<10	10	<10	<10	10	<10	20	<10	<10	<10	<10	20	<10
Zn	70	50	70	50	60	50	80	<30	40	70	60	70	70	40
Ga	23	24	22	19	27	20	26	16	16	21	18	21	19	20
Ge	1.6	2.3	1.7	1.6	1.9	1.8	1.6	1.6	1.8	1.8	1.9	1.6	1.8	1.8
As	<5	<5	<5	<5	<5	<5	29	<5	<5	11	<5	<5	<5	<5
Rb	247	246	204	212	265	205	316	163	220	235	234	192	145	213
Sr	202	30	244	185	28	72	90	74	224	136	111	357	403	101
Y	11.3	10.9	20.8	16.1	7.5	22.6	11.4	10.5	13.6	14.3	10.8	16.6	19.9	12.9
Zr	137	50	254	144	19	130	186	35	142	97	147	204	231	106
Nb	9.1	7.6	11.4	7.6	13	9.6	7.6	7.8	7.9	5.9	10.4	11.6	11.2	10.7
Mo	<2	<2	4	<2	3	<2	3	<2	4	<2	4	<2	2	<2
Ag	1.1	0.6	1	0.7	<0.5	0.6	0.7	<0.5	<0.5	<0.5	0.6	<0.5	0.7	<0.5
In	0.1	0.1	<0.1	0.1	0.3	0.1	0.2	<0.1	<0.1	0.1	0.1	<0.1	0.1	0.1
Sn	7	12	7	7	17	13	23	8	8	12	14	5	7	15
Sb	0.8	0.7	0.9	0.7	1	0.8	0.8	0.7	0.9	0.9	0.7	0.6	0.7	0.7
Cs	8.4	11.4	10.4	9.8	8	5	12.2	27.3	14.2	27.9	11	11.4	12.3	6.4
Ba	782	81	805	778	77	514	456	115	564	530	378	1263	1179	358
Hf	3.4	1.6	6.6	3.6	0.8	3.7	4.8	1.4	3.6	3.1	3.8	5.1	5.6	2.8
Ta	1.3	1.5	1.7	1.2	2.5	1.4	2.9	3.6	1.4	1.1	1.6	1.1	1.1	2.3
W	4.4	2.9	4.4	3.9	7.2	8.0	7.1	2.8	5.0	3.9	3.8	3.9	3.1	5.2
Tl	1.4	1.5	1.3	1.4	1.5	1.2	1.8	1.1	1.4	1.4	1.4	1.0	0.9	1.3
Pb	41.0	26.0	28.0	35.0	24.0	28.0	36.0	44.0	66.0	61.0	39.0	44.0	28.0	43.0
Bi	0.3	1.5	0.3	0.3	1.5	0.6	0.4	<0.1	0.1	0.5	0.2	0.1	0.2	0.8
Th	19.5	3.9	21.6	12.9	2.4	8.3	27.8	79.8	24.0	13.3	30.2	26.3	13.6	17.9
U	6.0	6.3	4.7	3.9	10.2	5.2	8.0	10.0	7.6	9.2	10.5	4.0	4.9	14.9
La	37.7	7.5	53.5	29.5	4.8	20.6	45.3	40.0	42.4	36.7	50.4	70.1	29.5	22.4
Ce	77.0	15.9	103.0	57.0	10.1	43.7	94.5	82.4	87.2	73.2	96.2	131.0	63.5	42.0
Pr	8.6	1.8	11.6	6.6	1.1	5.1	12.0	9.5	9.7	8.3	10.2	13.6	7.9	4.5
Nd	32.4	7.0	43.5	24.3	3.6	21.1	44.9	33.0	34.7	29.3	34.5	47.4	31.5	15.6
Sm	6.1	1.9	8.1	4.3	1.1	4.5	9.6	7.0	6.2	6.1	5.5	7.2	6.1	3.0
Eu	1.1	0.2	1.4	0.9	0.1	0.7	0.8	0.6	1.0	1.0	0.7	1.5	1.5	0.5
Gd	4.4	1.8	5.5	3.7	1.1	4.1	6.4	4.5	3.6	4.2	3.6	4.4	4.6	2.1
Tb	0.6	0.4	0.8	0.5	0.2	0.7	0.8	0.5	0.5	0.7	0.5	0.6	0.7	0.4
Dy	2.7	2.0	4.1	3.0	1.2	4.4	2.9	2.5	2.8	3.3	2.4	3.2	3.9	2.2
Ho	0.4	0.3	0.7	0.5	0.2	0.8	0.4	0.4	0.5	0.5	0.4	0.6	0.7	0.4
Er	0.9	0.8	1.9	1.6	0.7	2.3	0.9	1.0	1.3	1.3	1.1	1.6	2.1	1.2
Tm	0.1	0.1	0.3	0.2	0.1	0.3	0.1	0.1	0.2	0.2	0.2	0.2	0.3	0.2
Yb	0.7	0.9	1.6	1.4	0.8	2.0	0.7	0.8	1.2	1.1	1.3	1.4	1.8	1.4
Lu	0.1	0.1	0.3	0.2	0.1	0.3	0.1	0.1	0.2	0.2	0.2	0.2	0.3	0.2
LaN/LuN	38.85	6.37	21.96	14.83	4.60	7.12	52.45	33.24	25.40	22.92	26.91	39.47	11.09	10.74
Eu/Eu*	0.63	0.26	0.64	0.73	0.37	0.51	0.29	0.31	0.63	0.61	0.47	0.84	0.84	0.65

Note: LOI—loss on ignition. Major element concentrations in wt% oxide. Trace element concentrations in ppm. Fe as total FeO wt%. ASI—alumina saturation index (molar). *T*zirc—Zircon saturation temperature calculated based on Watson and Harrison (1983). ASI and *T*zirc values are not given for samples GP5, GP6, and GP9 because they are altered.

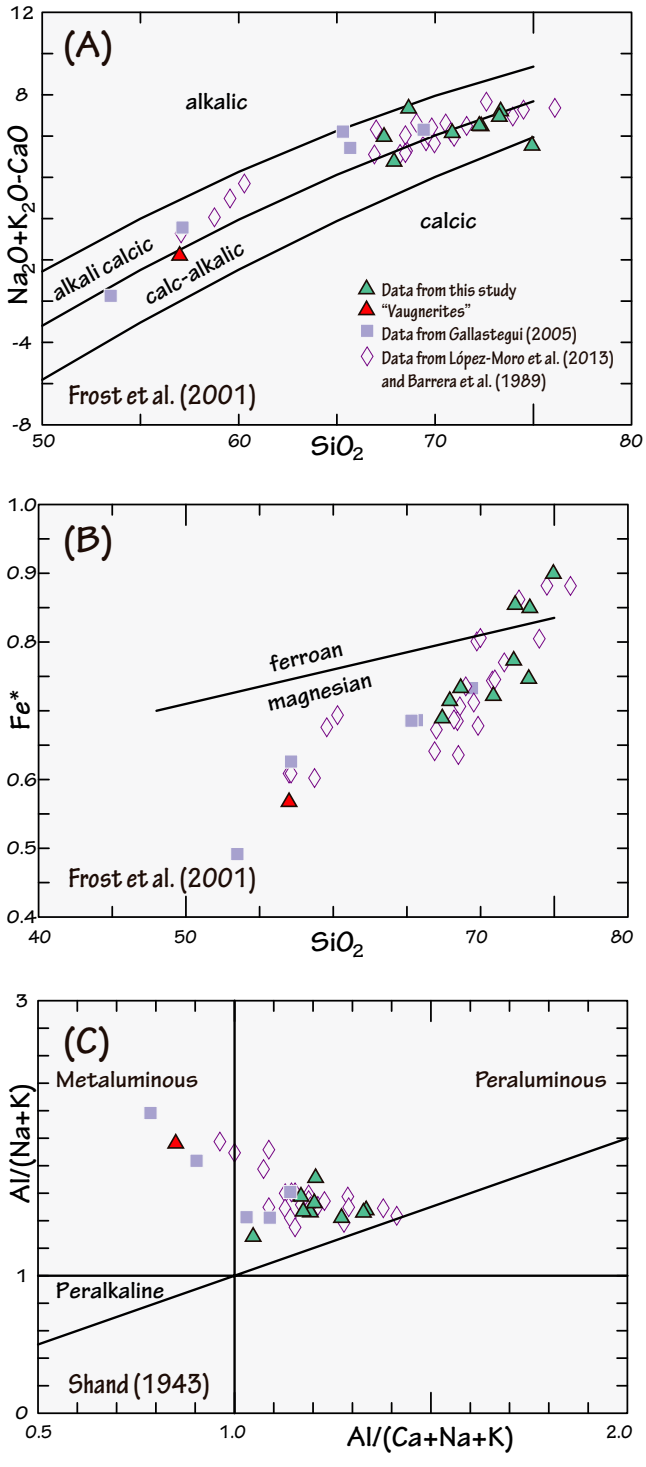

Figure 3. Geochemical features of the early Carboniferous suite (ECS) granitoids. (A) SiO_2 versus $Na_2O + K_2O$-CaO diagram of Frost et al. (2001). (B) SiO_2 versus $FeO^{total}/(FeO^{total} + MgO)$ diagram (Frost et al., 2001). (C) A/CNK (molar ratio of $Al_2O_3/CaO + Na_2O + K_2O$) versus A/NK diagram (Shand, 1943).

(for discussions on the occurrence, age, and genesis of durbachite and/or vaugnerite rocks in the Variscan belt of Europe, see Buda et al., 2004; Scarrow et al., 2009; von Raumer et al., 2014; Kubínová et al., 2017).

Figure 5 shows some aspects of a broad comparison between the ECS and the POS (Fernández-Suárez et al., 2000, 2011). This comparison is pertinent because both suites of granitoids are relatively similar in their main petrological and geochemical features (e.g., Capdevila et al., 1973; Fernández-Suárez et al., 2000) and both show associated mantle-derived mafic rocks, at variance with the syntectonic leucogranitoids that are associated with migmatites, and are the product synextensional melting of the middle crust (e.g., López Moro et al., 2018, and references therein).

Figure 5A shows a KDE (kernel density estimation) diagram of ASI values in samples from the ECS and the POS. Note that the peak of ASI values is ~1.05 in the POS and ~1.2 in the ECS. This is consistent with the involvement of a higher proportion of more aluminous rocks in the genesis of the ECS. This observation is also consistent with the trend defined by the ECS granitoids in the Ba-Zr diagram (Fig. 5B; Clemens, 2014) that is rather characteristic of S-type granitoids. For comparison, representative Ba-Zr analyses of the POS have been plotted in this diagram. Although both suites (ECS, POS) are not strikingly different in this diagram, the ECS seems to show a better positive correlation of Zr and Ba. As both suites are mainly crustal and likely derived from different admixtures of metaigneous and metasedimentary protolith rocks (see following), it makes sense that the plot does not show a clear-cut difference between them. This observation is consistent with the postulated more I-type nature of most granitoids belonging to the POS (Fernández-Suárez et al., 2011; see Villaseca et al., 1998, for a discussion on the significance of the I/S classification scheme in Iberian Variscan granitoids). The Th versus U diagram (Fig. 5C) shows that for similar whole-rock Th contents, the POS granitoids (with only two exceptions) have significantly lower whole-rock U contents; at face value, this is consistent with the involvement of a more pelitic (and hence more aluminous) source in the genesis of the ECS.

This apparent geochemical source-composition difference between the ECS and the POS is also evident in the different apparent zircon inheritance patterns of both suites (see following).

GEOCHRONOLOGY

We collected 13 samples corresponding to intrusions ascribed to the early granodiorite group in the regional literature (López-Plaza and Martínez Catalán 1987; Bellido Mulas et al., 1987; Gallastegui, 2005) for this study (location in Fig. 2). Among all samples, sample GP-1 (not reported herein) did not contain any early Carboniferous zircon and sample GP-9 was devoid of zircon. All but one zircon analyzed in sample GP-1 were older than ca. 480 Ma and therefore can be considered as inherited zircon crystals. In this sample only one Variscan concordant zircon was found, with an age of ca. 317 Ma. For this reason, sample GP-1 has been excluded from this study, as there is no evidence that it belongs to the ECS.

Analytical Procedures

Zircons were separated at the University of Salamanca (Spain); ~8 kg of sample were crushed in a jaw crusher and sieved for the 63-400 µm fraction. Concentrates were obtained using a Wilfley table, Frantz isodynamic magnetic separator, and heavy liquids (diiodomethane).

Zircon crystals of all grain sizes and morphological types were selected, mounted in resin blocks, and polished to half their thickness at the Museum für Mineralogie und Geologie (Senckenberg Naturhistorische Sammlungen Dresden) for subsequent analysis. All grains were documented by backscattered electron and cathodoluminescence (CL) images using a

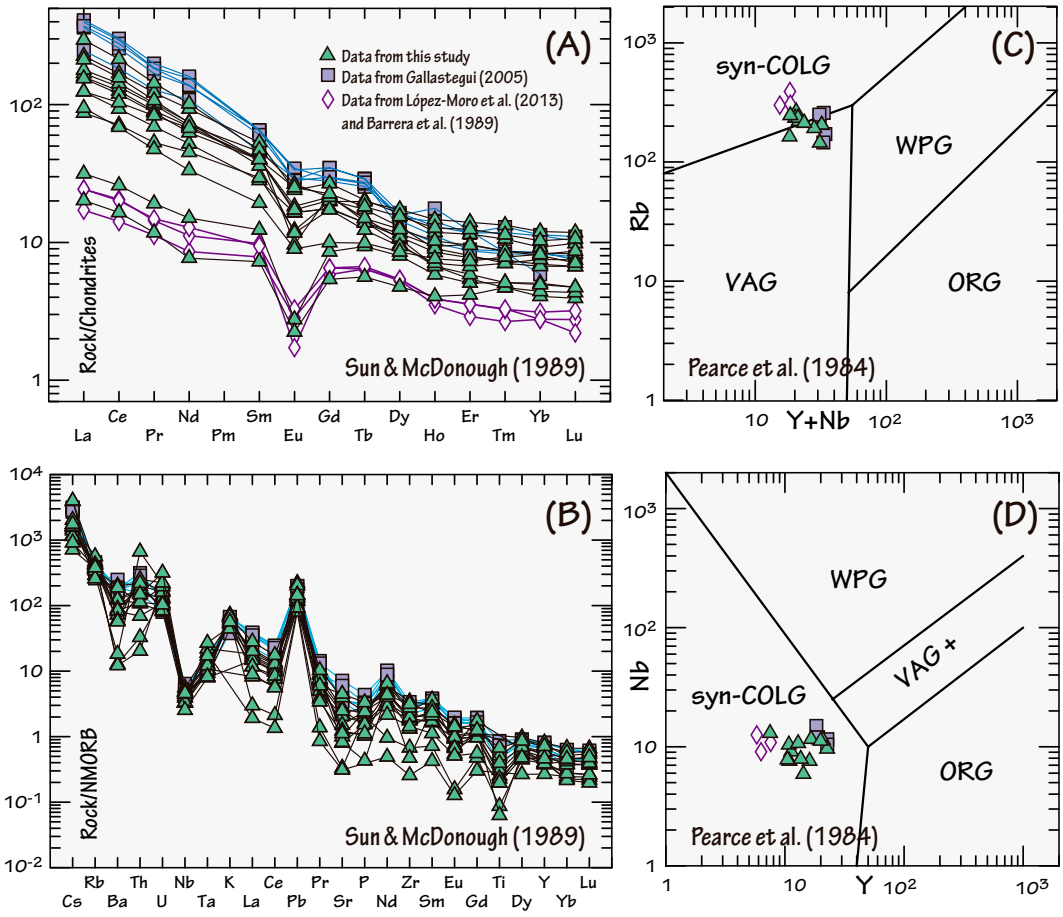

Figure 4. (A) Chondrite normalized rare earth element plot for the early Carboniferous suite (ECS) granitoids (normalization values of Sun and McDonough, 1989). (B) Normal mid-oceanic ridge basalt (N-MORB) normalized trace element plot for the ECS granitoids (normalization values of Sun and McDonough, 1989). (C) Rb versus Y + Nb tectonic discrimination diagram (Pearce et al., 1984). COLG—collision granites; VAG—volcanic arc granites; WPG—within plate granites; ORG—ocean ridge granites. (D) Y versus Nb tectonic discrimination diagram (Pearce et al., 1984).

scanning electron microscope (JEOL JSM-820 at the Research Assistance Centre of Geological Techniques, Complutense University, Madrid, Spain) to study their internal structure to select the best areas for laser ablation. Zircon was analyzed for U, Th, and Pb isotopes by LA-ICP-MS using a Thermo-Scientific Element 2 XR sector field ICP-MS coupled to a New Wave UP-193 excimer laser system. A teardrop-shaped, low-volume laser cell by Ben Jähne (Dresden, Germany) was used to enable sequential sampling of heterogeneous grains (e.g., growth zones) during time-resolved data acquisition. Each analysis consisted of ~15 s background acquisition followed by 35 s data acquisition, using a laser spot size of 25 µm. We analyzed 60 zircon crystals from each sample. If necessary, a common-Pb correction based on the interference- and background-corrected ^{204}Pb signal and a model Pb composition (Stacey and Kramers, 1975) was carried out. The necessity of the correction is judged on whether the corrected ^{207}Pb/^{206}Pb is outside of the internal errors of the measured ratios. Discordant analyses were generally discarded. Raw data were corrected for background signal, common Pb, laser-induced elemental fractionation, instrumental mass discrimination, and time-dependent elemental fractionation of Pb/Th and Pb/U using an Excel spreadsheet program developed by Axel Gerdes (Institute of Geosciences, Johann Wolfgang Goethe-University Frankfurt, Frankfurt am Main, Germany). Reported uncertainties were propagated by quadratic addition of the external reproducibility obtained from the standard zircon GJ-1 (~0.6% and 0.5%–1% for the ^{207}Pb/^{206}Pb and ^{206}Pb/^{238}U, respectively) during individual analytical sessions and the within-run precision of each analysis. Only concordant results (95%–105% concordance) were considered for single analysis. Concordia diagrams (2σ error ellipses) and concordia ages (95% confidence level) were produced using Isoplot/Ex 3.75 (Ludwig, 2012). (For further details on analytical protocol and data processing, see Frei and Gerdes, 2009.)

U-Pb Results: The Visean Event

Results of LA-ICP-MS U-Pb zircon analyses are listed in Table 2 and representative CL images of the analyzed zircons are shown in Figure 6. For the sake of clarity, we address first the results of U-Pb analyses interpreted to date the age of magmatic crystallization in each intrusion and then discuss the inherited zircon ages and inheritance patterns.

Figure 7 shows the Wetherill concordia diagrams obtained from the U-Pb data interpreted to represent the magmatic crystallization age of each intrusion. A summary of the obtained concordia ages and the number of analyses is shown in Table 3; the ages range from 347 to 337 Ma. Because several of the used samples were collected in the same pluton, there are some considerations.

Note that hitherto, in the regional literature the intrusions from which samples GP-3 and GP-4 were collected are considered to be a composite intrusion, but our results indicate that sample GP-3 is ~5 m.y. older than GP-4, so they are not, strictly speaking, coeval, although they form a continuous body of granitoid exposure (Fig. 2).

Samples GP-6 and GP-6A (Irixoa-Espenuca granite) were taken ~25 m apart. The results of U-Pb analyses of both samples are shown separately in Table 2, but the data have been combined in one concordia plot, as the analyses are equivalent and the pooled 17 analyses yield a concordia

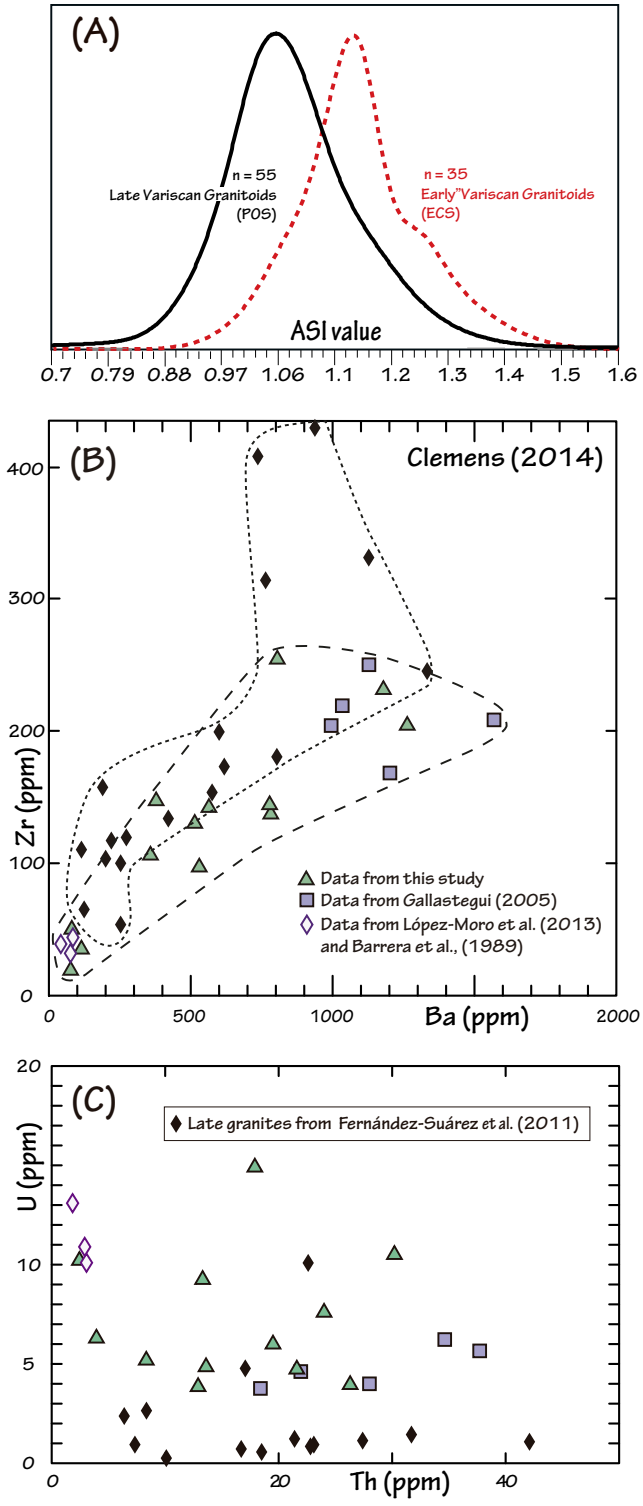

Figure 5. (A) Kernel density estimation plot (KDE) of ASI (molar $Al_2O_3 / Na_2O + K_2O + CaO$) values for the early Carboniferous suite (ECS) and the postorogenic granitoid suite (POS) (see text for details). The plot was constructed using the DensityPlotter 7.3 software (Vermeesch, 2012). (B) Ba versus Zr diagram (Clemens, 2014); see text for details. (C) Whole-rock U versus Th content for the ECS and the POS granitoids (see text for details).

age of 338.8 ± 2.0 Ma, considered to represent the crystallization age of this granitoid.

Although samples GP-5, GP-6, and GP-7 belong to what was previously considered a single intrusion (the Espenuca pluton; Ortega et al., 1994; Ortega, 1998), our data show that samples GP-5 and GP-6 yield the same age within analytical uncertainty (ca. 338 Ma), and sample GP-7 (Fig. 2) with a concordia age of 343.1 ± 2.6, is slightly older.

It is noteworthy that Figure 2 shows that samples GP-3, GP-4, GP-5, GP-6, and GP-7 represent the largest present-day outcrop of ECS granitoids in northwest Iberia, and taken as a whole seem to represent a large intrusion built over an apparent time span of ~5 m.y. (343–338 Ma).

Zircon Inheritance and Zircon Saturation Temperatures

The results of LA-ICP-MS U-Pb analyses older than ca. 347 Ma are considered to be inherited crystals in the studied samples. They are provided in Table 2, keyed to the corresponding sample reference number and summarized in Table 3. In addition, Figure 8 shows the concordia plots (Figs. 8A, 8B) of inherited zircons and the KDE plots (Fig. 8C).

Because the CL-guided analyses (Fig. 6) were aimed primarily at establishing crystallization ages for the studied intrusions, a few preliminary considerations are in order.

1. In zircons with a clear core-rim structure, some cores were analyzed (Fig. 6), but most cores were often avoided to maximize the number of ages corresponding to the magmatic event that generated the granitoid suite. In some cases, analyses performed on zircon centers with no observable core-rim structure yielded ages older than 347 Ma, and are thus interpreted to represent zircon xenocrysts incorporated into the magma.

2. The same approach was followed in every sample when selecting spot analyses.

3. Given the above, the inherited zircons found in the studied samples may be at best a broad proxy for the proportion of zircon xenocrysts, but do not necessarily provide an accurate datum for the proportion of the total inherited zircon component in a given sample.

4. The following discussion is solely based on concordant (or near concordant) analyses. Therefore, the weight of those zircons older than ca. 347 Ma that yielded discordant ages remains unknown.

Assuming that the real spectrum of inheritance may be different from that apparent from the concordant analyses obtained for each sample, as the methodological approach has been the same for all samples, we consider that comparative values of apparent inheritance between samples are still worth reporting and considering. A brief summary of the main inherited zircon results in each sample is shown in Table 3.

As regards U-Pb ages of inherited zircon in the studied samples, data are presented in Table 2, summarized in Table 3, and illustrated in Figure 8. Our data show that the inheritance pattern in the ECS as revealed by concordant analyses is characterized by the following age populations, from youngest to oldest: (1) ca. 400–390 Ma (4%), (2) ca. 490-470 (55%), (3) ca. 760–540 Ma (31%), (4) ca. 1500–900 Ma (6%), and (5) pre-Neoproterozoic (3%). Therefore ~85% of the apparent inherited population in the ECS is dominated by Ediacaran–Cryogenian zircon (31%) and early Paleozoic zircon (55%). In the northwest Iberian Variscan realm these ages correspond to well-known magmatic events (see Introduction) related to the Cadomian arc orogeny (e.g., Fernández-Suárez et al., 2011) and the Ollo de Sapo event related to the lithospheric thinning caused by the opening of the Rheic ocean (e.g., Murphy et al., 2006; Linnemann et al., 2008). Ollo de Sapo is the regional term for a thick succession of augen gneisses and porphyroid acid volcanics of Early Ordovician age that crop out in many sections of the Variscan belt in western Europe (e.g., Díez Montes et al., 2010; Montero et al., 2007, 2017, and references therein).

TABLE 2. U-Pb ANALYTICAL DATA

Sample	Analysis	U (ppm)	Pb (ppm)	Th/U	$^{206}Pb/^{204}Pb$	$^{207}Pb/^{235}U$	2σ (%)	$^{206}Pb/^{238}U$	2σ (%)	$^{207}Pb/^{206}Pb$	2σ (%)	**$^{206}Pb/^{238}U$**	**2σ (Ma)**	$^{207}Pb/^{235}U$	2σ (Ma)	$^{207}Pb/^{206}Pb$	2σ (Ma)	Concordance (%)
GP2	a29	858	60	2.06	13762	0.4042	2.9	0.05491	1.7	0.05338	2.4	**345**	**6**	345	9	345	55	100
GP2	a30	284	17	0.49	187	0.4067	8.8	0.05505	2.3	0.05359	8.5	**345**	**8**	347	26	354	192	98
GP2	a23	139	8	0.63	3518	0.4076	5.4	0.05509	2.2	0.05365	5.0	**346**	**7**	347	16	356	112	97
GP2	a28	583	39	1.38	1582	0.4077	4.1	0.05522	1.2	0.05355	4.0	**347**	**4**	347	12	352	90	98
GP2	a25	528	31	0.09	253	0.4121	6.4	0.05548	1.3	0.05388	6.3	**348**	**4**	350	19	366	141	95
GP2	a24	115	7	0.74	2874	0.4096	4.9	0.05554	1.3	0.05349	4.8	**348**	**4**	349	15	350	107	100
GP2	a3	1226	63	0.01	6844	0.4105	2.2	0.05603	1.6	0.05314	1.5	**351**	**6**	349	7	335	34	105
GP2	a2	1014	55	0.14	2777	0.4158	4.0	0.05606	2.2	0.05380	3.3	**352**	**8**	353	12	363	75	97
GP3	a54	99	5	0.55	4956	0.3905	4.2	0.05338	1.8	0.05306	3.8	**335**	**6**	335	12	332	87	101
GP3	a32	253	13	0.13	6587	0.3966	3.6	0.05376	1.9	0.05350	3.1	**338**	**6**	339	10	350	69	96
GP3	a47	75	4	0.49	3296	0.3986	5.4	0.05427	2.1	0.05327	5.0	**341**	**7**	341	16	340	113	100
GP3	a43	50	3	0.61	2013	0.3955	9.2	0.05432	2.5	0.05280	8.8	**341**	**8**	338	27	320	200	106
GP3	a2	97	6	0.61	403	0.3973	11.5	0.05436	1.2	0.05302	11.4	**341**	**4**	340	34	329	259	104
GP3	a25	126	7	0.54	3282	0.3955	5.0	0.05443	2.3	0.05270	4.4	**342**	**8**	338	14	316	101	108
GP3	a5	471	25	0.27	1255	0.4013	6.7	0.05453	2.0	0.05337	6.4	**342**	**7**	343	20	345	145	99
GP3	a23	235	13	0.35	6399	0.4029	3.9	0.05453	1.5	0.05359	3.6	**342**	**5**	344	11	354	81	97
GP3	a37	250	13	0.32	6235	0.4051	4.6	0.05456	1.6	0.05386	4.3	**342**	**5**	345	13	365	96	94
GP3	a17	161	10	1.00	5562	0.4042	4.3	0.05459	1.5	0.05370	4.1	**343**	**5**	345	13	359	91	96
GP3	a26	261	14	0.19	6889	0.3979	3.4	0.05461	2.1	0.05284	2.7	**343**	**7**	340	10	322	61	106
GP3	a38	123	6	0.23	3418	0.4061	4.4	0.05465	2.4	0.05389	3.7	**343**	**8**	346	13	366	83	94
GP3	a48	120	6	0.30	2531	0.4010	4.3	0.05466	1.9	0.05322	3.8	**343**	**6**	342	12	338	86	102
GP3	a29	123	7	0.64	3113	0.4057	4.3	0.05477	1.7	0.05372	3.9	**344**	**6**	346	13	359	89	96
GP3	a21	351	20	0.54	9282	0.4002	3.4	0.05480	1.5	0.05296	3.1	**344**	**5**	342	10	327	70	105
GP3	a12	129	7	0.43	3834	0.4003	3.9	0.05488	1.6	0.05290	3.6	**344**	**5**	342	12	325	82	106
GP3	a40	137	8	0.48	4061	0.4059	4.0	0.05491	1.6	0.05361	3.7	**345**	**5**	346	12	355	83	97
GP3	a1	270	14	0.21	9457	0.4022	5.1	0.05497	2.0	0.05307	4.7	**345**	**7**	343	15	332	106	104
GP3	a15	415	22	0.21	6174	0.4041	3.2	0.05501	2.3	0.05327	2.3	**345**	**8**	345	9	340	52	101
GP3	a6	203	12	0.70	6705	0.4010	3.2	0.05504	1.4	0.05283	3.0	**345**	**5**	342	9	322	67	107
GP3	a34	83	5	0.76	2255	0.4094	6.9	0.05505	1.7	0.05394	6.7	**345**	**6**	348	20	369	150	94
GP3	a24	211	13	0.87	5718	0.4075	3.7	0.05509	2.0	0.05365	3.1	**346**	**7**	347	11	356	70	97
GP3	a30	73	4	0.31	729	0.4076	10.9	0.05516	3.5	0.05359	10.3	**346**	**12**	347	32	354	232	98
GP3	a52	93	5	0.21	4675	0.4069	4.8	0.05521	2.1	0.05346	4.2	**346**	**7**	347	14	348	96	99
GP3	a18	74	4	0.51	2054	0.4082	5.0	0.05522	2.1	0.05360	4.5	**347**	**7**	348	15	354	102	98
GP3	a55	72	4	0.22	2478	0.4067	4.3	0.05524	2.2	0.05341	3.7	**347**	**7**	347	13	346	84	100
GP3	a41	211	11	0.10	6916	0.4045	3.7	0.05529	1.8	0.05306	3.2	**347**	**6**	345	11	331	72	105
GP3	a10	185	11	0.48	660	0.4088	12.9	0.05530	1.6	0.05361	12.8	**347**	**5**	348	39	355	290	98
GP3	a3	94	5	0.44	3018	0.4037	5.2	0.05532	2.1	0.05293	4.8	**347**	**7**	344	15	326	108	107
GP3	a51	72	4	0.93	3445	0.4032	4.7	0.05534	1.9	0.05285	4.3	**347**	**6**	344	14	322	97	108
GP3	a59	44	2	0.37	2895	0.4091	5.1	0.05534	1.8	0.05362	4.8	**347**	**6**	348	15	355	109	98
GP3	a11	259	15	0.50	5809	0.4080	3.8	0.05543	1.8	0.05339	3.4	**348**	**6**	347	11	345	76	101
GP3	a53	78	4	0.27	4259	0.4077	4.1	0.05545	1.6	0.05333	3.7	**348**	**5**	347	12	343	85	101
GP3	a4	74	4	0.41	2472	0.4102	5.1	0.05570	2.5	0.05341	4.5	**349**	**8**	349	15	346	102	101
GP4	a46	97	5	0.36	3553	0.3846	6.6	0.05261	2.4	0.05303	6.1	**331**	**8**	330	19	330	138	100
GP4	a55	142	7	0.40	2785	0.3884	3.7	0.05278	1.4	0.05337	3.4	**332**	**5**	333	11	345	77	96
GP4	a53	318	16	0.12	5716	0.3900	4.6	0.05328	1.7	0.05310	4.3	**335**	**6**	334	13	333	98	100
GP4	a59	225	14	1.17	11025	0.3907	3.0	0.05329	1.5	0.05317	2.7	**335**	**5**	335	9	336	60	100
GP4	a13	1082	54	0.12	2182	0.3885	5.3	0.05333	2.7	0.05283	4.6	**335**	**9**	333	15	322	104	104
GP4	a27	1278	65	0.23	2200.59	0.3902	3.1	0.05333	1.5	0.053067	2.7	**335**	**5**	335	9	332	62	101
GP4	a57	108	6	0.25	5206.54	0.3896	4.7	0.05334	1.8	0.052985	4.3	**335**	**6**	334	13	328	98	102
GP4	a39	392	20	0.22	5882.03	0.3936	4.2	0.05343	1.6	0.053424	3.9	**336**	**5**	337	12	347	88	97
GP4	a34	2263	112	0.02	5857.96	0.3914	2.4	0.05346	2.1	0.053094	1.3	**336**	**7**	335	7	333	29	101
GP4	a5	465	27	0.92	3108.39	0.3913	4.6	0.05346	3.1	0.053078	3.4	**336**	**10**	335	13	332	77	101
GP4	a48	192	10	0.52	9261.83	0.3942	3.1	0.05354	1.9	0.0534	2.4	**336**	**6**	337	9	346	54	97
GP4	a8	1675	94	0.32	7039.64	0.3902	2	0.05356	1.3	0.052838	1.5	**336**	**4**	335	6	322	35	105
GP4	a38	582	30	0.31	2739.6	0.3956	3.8	0.05358	1.6	0.053552	3.4	**336**	**5**	338	11	352	77	96
GP4	a31	936	46	0.05	20207.6	0.3889	2.2	0.05358	1.4	0.052637	1.7	**336**	**5**	334	6	313	39	107
GP4	a7	281	15	0.77	8881.57	0.3978	2.6	0.05371	1.2	0.053716	2.3	**337**	**4**	340	7	359	51	94
GP4	a47	569	28	0.08	23041.5	0.3929	2.4	0.05386	1.2	0.052901	2.1	**338**	**4**	336	7	325	48	104
GP4	a36	607	37	1.34	3533.34	0.3945	3.5	0.05390	1.7	0.053093	3.1	**338**	**5**	338	10	333	69	102
GP4	a54	787	40	0.10	2913.84	0.3932	2.3	0.05394	1.4	0.052865	1.9	**339**	**4**	337	7	323	42	105
GP4	a12	472	26	0.71	5881.65	0.3967	4.9	0.05399	1.4	0.053293	4.7	**339**	**5**	339	14	341	105	99
GP4	a14	451	25	0.72	4634.77	0.3955	4.1	0.05400	1.6	0.053121	3.7	**339**	**5**	338	12	334	85	102
GP4	a41	473	25	0.42	5276.48	0.3947	3.6	0.05402	1.3	0.052995	3.4	**339**	**4**	338	10	329	77	103
GP4	a60	176	9	0.10	2010.8	0.4000	4	0.05419	2.9	0.053531	2.8	**340**	**10**	342	12	351	63	97
GP4	a32	781	41	0.31	1622.62	0.3977	3.6	0.05423	1.2	0.053189	3.4	**340**	**4**	340	11	337	77	101
GP4	a9	365	22	1.01	13276.5	0.3984	3.1	0.05427	1.5	0.053245	2.7	**341**	**5**	340	9	339	61	100
GP4	a2	772	39	0.09	4497.61	0.4024	2.6	0.05428	1.4	0.053766	2.1	**341**	**5**	343	7	361	48	94

(*continued*)

TABLE 2. U-Pb ANALYTICAL DATA (*continued*)

Sample	Analysis	U (ppm)	Pb (ppm)	Th/U	$^{206}Pb/^{204}Pb$	$^{207}Pb/^{235}U$	2σ (%)	$^{206}Pb/^{238}U$	2σ (%)	$^{207}Pb/^{206}Pb$	2σ (%)	**$^{206}Pb/^{238}U$**	**2σ (Ma)**	$^{207}Pb/^{235}U$	2σ (Ma)	$^{207}Pb/^{206}Pb$	2σ (Ma)	Concordance (%)
GP4	a49	120	7	1.10	5442.7	0.3999	3.3	0.05430	1.4	0.053417	3.0	**341**	**5**	342	10	347	67	98
GP4	a24	298	19	1.29	9729.03	0.3978	3.8	0.05459	2.7	0.052861	2.6	**343**	**9**	340	11	323	58	106
GP4	a22	544	32	0.77	1330.73	0.4057	5.3	0.05503	2.6	0.053468	4.6	**345**	**9**	346	16	349	104	99
GP5	a41	848	42	0.14	3073.88	0.3863	3.8	0.05263	2.3	0.053241	3.1	**331**	**7**	332	11	339	70	97
GP5	a14	847	114	0.68	1287.04	0.3855	3.1	0.05302	1.6	0.052731	2.6	**333**	**5**	331	9	317	59	105
GP5	a16	598	30	0.15	2460.9	0.3932	4.3	0.05310	1.8	0.053702	3.9	**334**	**6**	337	12	359	88	93
GP5	a50	832	41	0.04	11640.9	0.3891	6.5	0.05319	4.7	0.053057	4.4	**334**	**15**	334	19	331	100	101
GP5	a26	1637	85	0.23	40743.1	0.3857	2.4	0.05327	1.7	0.052518	1.6	**335**	**6**	331	7	308	37	109
GP5	a10	988	119	0.57	4552.42	0.3940	4.7	0.05329	2.4	0.053627	4.0	**335**	**8**	337	14	355	91	94
GP5	a21	596	31	0.25	2655.55	0.3891	3.6	0.05332	2.5	0.052925	2.6	**335**	**8**	334	10	326	59	103
GP5	a33	585	30	0.20	2872.59	0.3922	5.5	0.05337	1.4	0.053306	5.3	**335**	**5**	336	16	342	120	98
GP5	a12	756	74	0.61	14891.1	0.3939	2.6	0.05342	1.9	0.053485	1.7	**335**	**6**	337	7	349	38	96
GP5	a17	1390	69	0.08	4451.69	0.3898	2.7	0.05349	1.5	0.052856	2.2	**336**	**5**	334	8	323	51	104
GP5	a13	268	14	0.22	7947.01	0.3940	5.1	0.05352	3.8	0.053393	3.3	**336**	**12**	337	15	346	76	97
GP5	a55	193	19	1.43	579.683	0.3906	8.7	0.05357	2.2	0.052878	8.4	**336**	**7**	335	25	324	191	104
GP5	a31	779	39	0.09	8878.68	0.3958	3.1	0.05371	1.7	0.053453	2.6	**337**	**6**	339	9	348	58	97
GP5	a29	1245	91	0.75	5525.99	0.3904	4.6	0.05371	2.4	0.052724	3.9	**337**	**8**	335	13	317	88	106
GP5	a20	692	36	0.38	14814.3	0.3950	2.7	0.05382	1.9	0.053224	1.9	**338**	**6**	338	8	338	44	100
GP5	a58	83	5	0.48	5607.1	0.3928	4.6	0.05392	3.1	0.052831	3.3	**339**	**10**	336	13	322	75	105
GP5	a34	681	37	0.25	816.03	0.3954	6	0.05394	2.1	0.053166	5.6	**339**	**7**	338	17	336	128	101
GP5	a54	97	6	1.37	6111.56	0.3999	3.6	0.05394	1.9	0.053766	3.0	**339**	**6**	342	10	361	68	94
GP5	a32	1839	93	0.10	19227.5	0.3923	2.7	0.05397	1.8	0.052717	2.0	**339**	**6**	336	8	317	46	107
GP5	a6	501	25	0.08	15519.1	0.3955	2.6	0.05401	1.7	0.053112	1.9	**339**	**6**	338	7	334	44	102
GP5	a51	186	10	0.21	1862.95	0.4014	5.1	0.05404	2.6	0.053865	4.3	**339**	**9**	343	15	365	98	93
GP5	a42	641	32	0.13	22135.3	0.4009	3.5	0.05405	2.6	0.053799	2.4	**339**	**9**	342	10	363	53	94
GP5	a8	593	38	0.96	19276.7	0.3957	4.7	0.05408	2.9	0.053064	3.8	**340**	**9**	339	14	332	86	102
GP5	a30	611	32	0.33	6252.13	0.4016	3.5	0.05418	2.2	0.053761	2.7	**340**	**7**	343	10	361	62	94
GP5	a48	449	26	0.47	4361.12	0.4000	2.9	0.05419	1.6	0.053532	2.4	**340**	**5**	342	8	351	54	97
GP5	a27	617	32	0.08	1678.85	0.4044	4	0.05422	3.2	0.0541	2.4	**340**	**11**	345	12	375	54	91
GP5	a35	644	32	0.03	17362	0.3943	2.7	0.05425	1.6	0.052704	2.2	**341**	**5**	337	8	316	50	108
GP5	a49	355	19	0.35	790.068	0.4021	4.4	0.05436	2.6	0.053637	3.6	**341**	**9**	343	13	356	82	96
GP5	a57	67	4	0.54	2032.78	0.4028	5.1	0.05438	3.0	0.053716	4.1	**341**	**10**	344	15	359	93	95
GP5	a9	585	31	0.30	989.237	0.4047	3.4	0.05459	2.3	0.05377	2.5	**343**	**8**	345	10	361	56	95
GP5	a4	1239	63	0.11	3826.8	0.4029	4.5	0.05487	2.0	0.053261	4.0	**344**	**7**	344	13	340	92	101
GP6	a38	106	6	0.54	701.396	0.3857	12	0.05264	2.6	0.053151	11.5	**331**	**8**	331	34	335	260	99
GP6	a47	139	7	0.11	6288.95	0.3939	4.5	0.05348	2.8	0.053418	3.4	**336**	**9**	337	13	347	78	97
GP6	a23	305	16	0.12	1125.23	0.3925	7.5	0.05358	3.4	0.053121	6.6	**336**	**11**	336	22	334	150	101
GP6	a36	514	26	0.03	2360.71	0.4003	5.9	0.05396	1.5	0.053803	5.7	**339**	**5**	342	17	363	128	93
GP6	a2	1251	62	0.03	6901.92	0.4008	2.9	0.05422	1.7	0.053611	2.3	**340**	**6**	342	8	355	51	96
GP6	a46	127	7	0.19	833.097	0.4006	6.8	0.05445	3.5	0.053365	5.9	**342**	**12**	342	20	344	133	99
GP6	a12	182	9	0.08	3852.67	0.4081	7.2	0.05514	4.8	0.053677	5.4	**346**	**16**	347	21	358	122	97
GP6A	a58	370	19	0.27	3550.54	0.3944	3	0.05339	1.9	0.053575	2.3	**335**	**6**	338	9	353	53	95
GP6A	a41	878	65	0.71	1376.48	0.3936	4.5	0.05364	2.9	0.053219	3.5	**337**	**10**	337	13	338	78	100
GP6A	a42	444	24	0.32	1177.28	0.3980	7.8	0.05373	2.0	0.053727	7.6	**337**	**7**	340	23	360	171	94
GP6A	a56	407	21	0.16	22013.1	0.3957	4	0.05387	2.1	0.053276	3.4	**338**	**7**	339	11	341	76	99
GP6A	a54	457	36	0.76	678.859	0.3966	4.6	0.05396	2.3	0.053313	4.0	**339**	**8**	339	13	342	90	99
GP6A	a48	380	20	0.31	2844.49	0.4016	4.5	0.05426	3.3	0.053679	3.0	**341**	**11**	343	13	358	68	95
GP6A	a49	205	10	0.04	5261.13	0.3989	7.9	0.05435	3.6	0.053229	7.0	**341**	**12**	341	23	339	159	101
GP6A	a45	60	3	0.24	1765.27	0.3991	6.4	0.05450	3.5	0.053114	5.4	**342**	**12**	341	19	334	122	103
GP6A	a60	78	4	0.81	4192.53	0.4061	9.5	0.05498	2.3	0.053571	9.2	**345**	**8**	346	28	353	209	98
GP6A	a50	485	25	0.03	2604.75	0.4072	7.5	0.05531	4.0	0.053389	6.3	**347**	**13**	347	22	345	143	100
GP7	a31	3043	159	0.28	1759.89	0.3999	7.3	0.05415	1.9	0.05356	7.0	**340**	**6**	342	21	353	158	96
GP7	a16	88	6	0.73	452.172	0.3964	14	0.05432	3.8	0.052925	13.7	**341**	**13**	339	42	326	310	105
GP7	a15	1087	670	0.59	906.032	0.4011	2.7	0.05476	0.9	0.05312	2.6	**344**	**3**	342	8	334	58	103
GP7	a4	4164	216	0.14	2897.98	0.4048	4.3	0.05477	2.8	0.053611	3.3	**344**	**9**	345	13	355	75	97
GP7	a36	79	5	0.51	1667.18	0.4063	12	0.05499	2.8	0.053591	11.5	**345**	**9**	346	35	354	260	97
GP8	a20	426	25	0.76	550.954	0.3879	4.9	0.05285	1.8	0.053237	4.6	**332**	**6**	333	14	339	104	98
GP8	a44	689	34	0.10	17636.9	0.3845	2.7	0.05285	1.5	0.052768	2.2	**332**	**5**	330	8	319	51	104
GP8	a19	309	19	1.20	2499.73	0.3889	5.6	0.05304	1.9	0.053177	5.3	**333**	**6**	334	16	336	120	99
GP8	a59	442	22	0.15	26311.3	0.3904	3.4	0.05313	2.0	0.053296	2.8	**334**	**6**	335	10	341	63	98
GP8	a15	807	43	0.51	19332.6	0.3914	2.7	0.05326	1.9	0.053301	2.0	**335**	**6**	335	8	342	45	98
GP8	a54	184	11	1.03	3749.48	0.3907	5.5	0.05341	1.8	0.053055	5.2	**335**	**6**	335	16	331	118	101
GP8	a4	517	33	1.11	393.451	0.3901	6	0.05346	1.5	0.052919	5.8	**336**	**5**	334	17	325	133	103
GP8	a11	613	33	0.47	16908.4	0.3926	2.4	0.05352	1.6	0.053195	1.8	**336**	**5**	336	7	337	41	100
GP8	a25	1576	85	0.25	640.238	0.3932	4.5	0.05355	1.3	0.053255	4.3	**336**	**4**	337	13	340	98	99

(*continued*)

TABLE 2. U-Pb ANALYTICAL DATA (*continued*)

Sample	Analysis	U (ppm)	Pb (ppm)	Th/U	$^{206}Pb/^{204}Pb$	$^{207}Pb/^{235}U$	2σ (%)	$^{206}Pb/^{238}U$	2σ (%)	$^{207}Pb/^{206}Pb$	2σ (%)	**$^{206}Pb/^{238}U$**	**2σ (Ma)**	$^{207}Pb/^{235}U$	2σ (Ma)	$^{207}Pb/^{206}Pb$	2σ (Ma)	Concordance (%)
GP8	a26	1110	57	0.14	1496.92	0.3926	3.7	0.05359	2.1	0.053137	3.1	**337**	**7**	336	11	335	70	101
GP8	a28	250	15	1.15	2966.3	0.3927	6.2	0.05360	1.1	0.053147	6.1	**337**	**4**	336	18	335	139	100
GP8	a23	1234	64	0.17	1709.77	0.3938	4.4	0.05360	2.5	0.053287	3.7	**337**	**8**	337	13	341	83	99
GP8	a30	895	47	0.32	7406.3	0.3939	2.9	0.05361	1.7	0.053294	2.4	**337**	**6**	337	8	341	54	99
GP8	a58	194	11	0.79	12406.3	0.3896	3.2	0.05362	1.9	0.052692	2.5	**337**	**6**	334	9	316	57	107
GP8	a56	1143	57	0.05	7289.92	0.3936	3.8	0.05368	1.9	0.053182	3.3	**337**	**6**	337	11	337	75	100
GP8	a16	206	13	1.75	5085.58	0.3938	3.6	0.05371	1.4	0.053178	3.3	**337**	**5**	337	11	336	76	100
GP8	a57	590	30	0.15	3742.55	0.3914	2.3	0.05379	1.3	0.052778	1.9	**338**	**4**	335	7	319	43	106
GP8	a47	290	19	1.19	255.543	0.3974	5.5	0.05380	1.5	0.053582	5.3	**338**	**5**	340	16	354	120	96
GP8	a24	456	25	0.49	5219.03	0.3936	6.1	0.05382	1.1	0.053042	6.0	**338**	**4**	337	18	331	135	102
GP8	a34	876	49	0.59	946.445	0.3955	5.2	0.05393	1.0	0.053181	5.1	**339**	**3**	338	15	337	116	101
GP8	a41	439	27	1.18	12742.8	0.3987	2.9	0.05397	1.2	0.053577	2.6	**339**	**4**	341	8	353	59	96
GP8	a38	420	27	1.46	2717.54	0.3955	6.6	0.05401	2.0	0.053114	6.3	**339**	**7**	338	19	334	142	102
GP8	a6	205	13	1.13	5136.7	0.3955	6	0.05404	1.8	0.05308	5.8	**339**	**6**	338	17	332	130	102
GP8	a42	668	46	2.03	21213.5	0.3971	2	0.05417	1.1	0.053165	1.7	**340**	**4**	340	6	336	38	101
GP8	a27	777	46	0.88	1374.59	0.4007	3.8	0.05420	1.6	0.053618	3.5	**340**	**5**	342	11	355	79	96
GP8	a60	170	11	1.53	5992.16	0.3973	4.5	0.05423	2.0	0.053136	4.0	**340**	**7**	340	13	335	91	102
GP8	a45	414	26	1.12	16548.6	0.4031	2.4	0.05429	1.5	0.053848	1.9	**341**	**5**	344	7	365	42	93
GP8	a32	763	42	0.61	5838.79	0.3971	3.1	0.05430	1.3	0.053044	2.7	**341**	**4**	340	9	331	62	103
GP8	a52	247	15	0.75	1052.63	0.3969	3.8	0.05438	2.2	0.052937	3.1	**341**	**7**	339	11	326	71	105
GP8	a51	386	25	1.39	759.897	0.4023	5.2	0.05439	2.6	0.053643	4.5	**341**	**9**	343	15	356	101	96
GP10	a6	1514	77	0.12	3856.77	0.3952	4.7	0.05392	2.5	0.053157	4.0	**339**	**8**	338	14	335	90	101
GP10	a46	884	46	0.25	5027.04	0.3969	4.5	0.05413	1.5	0.053172	4.2	**340**	**5**	339	13	336	95	101
GP10	a4	529	31	0.70	6754.21	0.3997	5.4	0.05428	1.8	0.05341	5.1	**341**	**6**	341	16	346	116	98
GP10	a9	914	59	1.03	404.133	0.3975	6	0.05429	2.5	0.053113	5.4	**341**	**8**	340	17	334	123	102
GP10	a5	991	52	0.22	4948.58	0.4047	2.8	0.05442	2.0	0.053925	2.1	**342**	**7**	345	8	368	46	93
GP10	a12	585	40	1.80	1751.24	0.4053	4.1	0.05450	1.5	0.053938	3.8	**342**	**5**	345	12	368	86	93
GP10	a59	256	15	1.15	2650.42	0.4014	6	0.05450	2.0	0.053414	5.6	**342**	**7**	343	17	346	127	99
GP10	a48	465	25	0.36	18889.2	0.4042	2.9	0.05456	1.6	0.053729	2.5	**342**	**5**	345	9	360	56	95
GP10	a35	1413	73	0.16	8895.76	0.4026	2	0.05467	1.2	0.053409	1.6	**343**	**4**	344	6	346	36	99
GP10	a11	277	16	0.71	1574.52	0.4032	6.1	0.05475	1.9	0.053406	5.8	**344**	**6**	344	18	346	132	99
GP10	a58	1301	67	0.14	7395.53	0.4010	2.9	0.05478	1.8	0.053084	2.3	**344**	**6**	342	8	332	52	103
GP10	a50	315	19	1.08	12425.2	0.4032	3.5	0.05479	1.7	0.05338	3.1	**344**	**6**	344	10	345	70	100
GP10	a44	1401	75	0.37	844.687	0.4022	6.6	0.05482	2.9	0.053214	5.9	**344**	**10**	343	19	338	134	102
GP10	a17	487	26	0.32	3992.42	0.4030	4.3	0.05483	1.4	0.053316	4.0	**344**	**5**	344	12	342	91	101
GP10	a51	138	8	0.62	698.842	0.4065	11	0.05484	2.4	0.053753	10.9	**344**	**8**	346	33	361	246	95
GP10	a38	1342	69	0.16	11198.8	0.4025	2.3	0.05488	1.8	0.053199	1.5	**344**	**6**	343	7	337	34	102
GP10	a18	1700	88	0.17	6985.86	0.4043	4	0.05495	2.6	0.053358	3.1	**345**	**9**	345	12	344	70	100
GP10	a15	583	33	0.65	10598.6	0.4066	4.4	0.05496	1.8	0.053653	4.0	**345**	**6**	346	13	356	91	97
GP10	a8	363	24	1.99	9353.45	0.4054	2.7	0.05499	1.6	0.053469	2.2	**345**	**5**	346	8	349	50	99
GP10	a13	231	14	0.73	1069.33	0.4015	9.5	0.05501	2.7	0.05293	9.1	**345**	**9**	343	28	326	207	106
GP10	a47	559	31	0.40	2921.77	0.4030	4.4	0.05506	2.3	0.053087	3.8	**346**	**8**	344	13	333	85	104
GP10	a7	465	25	0.29	4477.01	0.4050	3.9	0.05507	2.5	0.053337	3.0	**346**	**8**	345	12	343	69	101
GP10	a23	705	46	1.29	833.047	0.4068	5.4	0.05508	3.5	0.053573	4.1	**346**	**12**	347	16	353	92	98
GP10	a3	563	33	0.92	4181.54	0.4053	4.2	0.05509	2.9	0.053364	3.0	**346**	**10**	346	12	344	67	100
GP10	a52	844	44	0.20	5232.62	0.4101	3.1	0.05512	2.6	0.053964	1.7	**346**	**9**	349	9	370	38	94
GP10	a55	667	36	0.25	1851.29	0.4027	3.7	0.05520	1.3	0.05291	3.5	**346**	**4**	344	11	325	79	107
GP10	a26	1233	70	0.79	4370.7	0.4034	2.9	0.05525	1.4	0.052956	2.5	**347**	**5**	344	8	327	57	106
GP10	a53	665	37	0.34	6584.21	0.4053	2.8	0.05540	1.7	0.053058	2.3	**348**	**6**	345	8	331	52	105
GP10	a60	961	49	0.05	6335.02	0.4063	2.4	0.05541	1.6	0.05318	1.8	**348**	**5**	346	7	336	40	103
GP10	a30	1512	78	0.10	3667.81	0.4110	1.7	0.05542	1.2	0.053788	1.3	**348**	**4**	350	5	362	28	96
GP10	a1	734	40	0.26	650.543	0.4111	7.1	0.05560	3.6	0.053626	6.1	**349**	**12**	350	21	355	138	98
GP10	a39	292	18	0.87	953.395	0.4144	6.3	0.05560	1.4	0.054054	6.1	**349**	**5**	352	19	373	138	93
GP10	a24	489	30	0.88	732.351	0.4075	5.8	0.05561	2.5	0.053142	5.2	**349**	**8**	347	17	335	118	104
GP10	a37	1610	87	0.15	1521.37	0.4089	4.1	0.05573	1.7	0.053212	3.8	**350**	**6**	348	12	338	85	103
GP10	a45	418	25	0.40	372.31	0.4139	5.1	0.05594	2.8	0.05367	4.3	**351**	**10**	352	15	357	97	98
GP11	a59	620	31	0.10	5326.05	0.3849	4.7	0.05266	3.1	0.053009	3.4	**331**	**10**	331	13	329	78	101
GP11	a43	403	21	0.26	9625.3	0.3877	3.2	0.05273	1.8	0.053326	2.6	**331**	**6**	333	9	343	59	97
GP11	a47	463	30	1.55	12888.7	0.3888	2.8	0.05292	1.2	0.053276	2.5	**332**	**4**	333	8	341	57	98
GP11	a60	272	15	0.64	661.241	0.3906	8.1	0.05303	2.2	0.053423	7.7	**333**	**7**	335	23	347	175	96
GP11	a53	278	15	0.43	3413.84	0.3896	6.7	0.05305	1.4	0.053263	6.5	**333**	**5**	334	19	340	148	98
GP11	a46	424	27	1.04	431.894	0.3913	11	0.05307	1.4	0.053471	10.5	**333**	**5**	335	31	349	237	96
GP11	a33	1315	66	0.09	1975.91	0.3863	4.7	0.05307	1.8	0.052786	4.3	**333**	**6**	332	13	320	98	104
GP11	a32	651	33	0.21	5800.25	0.3924	5	0.05313	1.5	0.053565	4.8	**334**	**5**	336	14	353	107	95
GP11	a29	968	51	0.29	2244.09	0.3885	8	0.05317	2.5	0.052986	7.6	**334**	**8**	333	23	328	173	102
GP11	a28	794	42	0.41	13974.5	0.3905	2.5	0.05323	1.1	0.053207	2.3	**334**	**4**	335	7	338	52	99
GP11	a6	429	22	0.25	10353.4	0.3902	3	0.05324	1.4	0.053165	2.7	**334**	**5**	335	9	336	60	100

(*continued*)

TABLE 2. U-Pb ANALYTICAL DATA (*continued*)

Sample	Analysis	U (ppm)	Pb (ppm)	Th/U	$^{206}Pb/^{204}Pb$	$^{207}Pb/^{235}U$	2σ (%)	$^{206}Pb/^{238}U$	2σ (%)	$^{207}Pb/^{206}Pb$	2σ (%)	**$^{206}Pb/^{238}U$**	**2σ (Ma)**	$^{207}Pb/^{235}U$	2σ (Ma)	$^{207}Pb/^{206}Pb$	2σ (Ma)	Concordance (%)
GP11	a55	354	18	0.24	1632.97	0.3915	4.6	0.05324	1.4	0.053327	4.4	**334**	**5**	335	13	343	100	98
GP11	a18	1265	66	0.32	5986.88	0.3869	6.6	0.05329	2.2	0.052654	6.2	**335**	**7**	332	19	314	142	107
GP11	a37	747	41	0.58	6092.24	0.3905	7.5	0.05331	3.7	0.053132	6.6	**335**	**12**	335	22	334	149	100
GP11	a49	383	21	0.43	3988.28	0.3907	4.7	0.05331	1.2	0.053155	4.5	**335**	**4**	335	13	335	102	100
GP11	a39	600	31	0.25	6646.2	0.3915	5.6	0.05341	3.4	0.053163	4.5	**335**	**11**	335	16	336	102	100
GP11	a27	403	23	0.64	2141.02	0.3893	11	0.05344	1.5	0.052832	10.9	**336**	**5**	334	32	322	247	104
GP11	a57	322	17	0.22	8894.81	0.3894	4.9	0.05345	2.0	0.052837	4.5	**336**	**7**	334	14	322	102	104
GP11	a12	1091	56	0.10	1069.32	0.3901	3.6	0.05346	1.5	0.052923	3.3	**336**	**5**	334	10	325	74	103
GP11	a21	485	32	1.32	1110.71	0.3908	6.5	0.05348	2.1	0.052995	6.1	**336**	**7**	335	19	329	138	102
GP11	a24	1068	57	0.35	1732.53	0.3885	3.1	0.05352	1.1	0.052649	2.9	**336**	**4**	333	9	314	67	107
GP11	a3	323	20	1.05	1693.02	0.3968	6.3	0.05364	1.5	0.053642	6.1	**337**	**5**	339	18	356	138	95
GP11	a58	344	19	0.40	1228.14	0.3951	4.2	0.05365	1.0	0.053414	4.1	**337**	**3**	338	12	346	93	97
GP11	a52	370	20	0.41	815.308	0.3946	5.8	0.05366	1.6	0.053331	5.5	**337**	**5**	338	17	343	126	98
GP11	a14	730	39	0.41	16444.4	0.3895	3.2	0.05368	2.3	0.052623	2.1	**337**	**8**	334	9	313	49	108
GP11	a50	388	24	1.14	2971.9	0.3962	4.9	0.05383	1.4	0.053388	4.7	**338**	**4**	339	14	345	107	98
GP11	a40	760	50	1.47	995.713	0.3904	4.8	0.05383	1.3	0.052604	4.7	**338**	**4**	335	14	312	106	108
GP11	a4	611	33	0.48	13943.2	0.3937	2.5	0.05384	1.3	0.053038	2.2	**338**	**4**	337	7	330	49	102
GP11	a41	487	26	0.25	779.15	0.3945	7.2	0.05394	2.1	0.053037	6.9	**339**	**7**	338	21	330	156	103
GP11	a9	885	46	0.28	5272.39	0.3968	3.5	0.05397	1.4	0.053319	3.2	**339**	**5**	339	10	342	72	99
GP11	a10	276	16	0.77	3466.26	0.3972	6.4	0.05402	1.5	0.05333	6.2	**339**	**5**	340	19	343	141	99
GP11	a34	3157	158	0.06	14320.7	0.3944	2.4	0.05415	1.1	0.052819	2.2	**340**	**4**	338	7	321	50	106
GP11	a1	842	43	0.16	9659.61	0.3966	2.4	0.05417	1.0	0.053101	2.1	**340**	**3**	339	7	333	48	102
GP11	a31	507	30	0.98	4073.35	0.3969	6	0.05437	1.6	0.052952	5.8	**341**	**5**	339	18	327	132	104
GP11	a26	1159	81	1.60	1292.71	0.4026	4	0.05438	2.2	0.053699	3.3	**341**	**7**	344	12	358	76	95
GP11	a13	605	31	0.17	8398.82	0.4015	3.5	0.05438	1.8	0.053546	2.9	**341**	**6**	343	10	352	66	97
GP11	a5	638	33	0.09	1320.7	0.4042	6	0.05440	1.8	0.053886	5.8	**341**	**6**	345	18	366	130	93
GP11	a42	375	21	0.30	915.108	0.3969	4.1	0.05446	2.1	0.052862	3.6	**342**	**7**	339	12	323	82	106
GP11	a54	382	22	0.74	2949.71	0.3997	5.8	0.05448	1.9	0.053204	5.5	**342**	**6**	341	17	337	124	101
GP11	a36	639	35	0.45	6004.56	0.4013	3	0.05452	1.6	0.053386	2.5	**342**	**5**	343	9	345	56	99
GP11	a48	129	7	0.63	3867.82	0.4027	3.8	0.05456	1.9	0.05353	3.3	**342**	**6**	344	11	351	75	97
GP-12	a3	2515	134	0.49	1271.62	0.3944	3.2	0.05388	1.5	0.05308	2.8	**338**	**5**	338	9	332	63	102
GP-12	a8	2514	134	0.44	12976.1	0.3897	2.1	0.05373	1.6	0.0526	1.6	**337**	**5**	334	6	311	31	108
GP12	b49	666	36	0.42	2812.97	0.3877	3.4	0.05335	1.5	0.052703	3.0	**335**	**5**	333	10	316	69	106
GP12	b57	458	24	0.35	2058.53	0.3954	2.6	0.05336	1.0	0.053749	2.4	**335**	**3**	338	8	361	54	93
GP12	b54	378	19	0.08	18385.7	0.3954	2.4	0.05348	1.5	0.053623	1.9	**336**	**5**	338	7	355	43	95
GP12	b36	1545	79	0.13	2755.89	0.3960	4.5	0.05354	2.3	0.053648	3.8	**336**	**8**	339	13	356	87	94
GP12	b19	911	47	0.20	4425.94	0.3926	4.9	0.05356	4.1	0.05316	2.6	**336**	**13**	336	14	336	60	100
GP12	b51	829	46	0.72	2988.65	0.3940	3.3	0.05361	2.1	0.053299	2.6	**337**	**7**	337	10	342	59	99
GP12	b53	383	19	0.07	11527.2	0.3948	2.7	0.05363	1.9	0.053383	2.0	**337**	**6**	338	8	345	45	98
GP12	b31	1283	65	0.09	4049.76	0.3917	5.1	0.05366	3.0	0.052942	4.2	**337**	**10**	336	15	326	95	103
GP12	b29	997	56	0.61	1359.17	0.3947	3	0.05373	1.5	0.053272	2.6	**337**	**5**	338	9	340	58	99
GP12	b35	778	38	0.03	18539.2	0.3937	2.7	0.05385	1.6	0.053031	2.2	**338**	**5**	337	8	330	50	102
GP12	b43	692	36	0.25	3657.59	0.3937	2.7	0.05386	1.5	0.053009	2.3	**338**	**5**	337	8	329	52	103
GP12	b38	656	34	0.71	2661.04	0.3920	4.8	0.05393	2.1	0.052724	4.3	**339**	**7**	336	14	317	99	107
GP12	b45	941	59	1.05	13523.3	0.3960	3	0.05393	1.7	0.053254	2.5	**339**	**6**	339	9	340	56	100
GP12	b48	413	22	0.19	3512.05	0.4016	3.2	0.05403	1.9	0.053907	2.6	**339**	**6**	343	9	367	59	92
GP12	b21	411	22	0.30	8720.41	0.3973	2.8	0.05406	1.4	0.053306	2.4	**339**	**5**	340	8	342	55	99
GP12	b26	770	39	0.08	3921.83	0.4002	3	0.05419	1.8	0.053556	2.4	**340**	**6**	342	9	352	54	97
GP12	b56	414	21	0.07	2852.75	0.3963	3.2	0.05423	2.1	0.053004	2.4	**340**	**7**	339	9	329	55	103
GP12	b47	1378	74	0.38	4006.36	0.3953	4	0.05428	3.1	0.052826	2.6	**341**	**10**	338	12	321	58	106
GP12	b20	465	24	0.13	13321.3	0.4008	2.9	0.05428	1.6	0.053554	2.3	**341**	**5**	342	8	352	53	97
GP12	b27	1024	56	0.41	2624.49	0.3983	3.3	0.05433	1.9	0.05317	2.7	**341**	**6**	340	10	336	62	101
GP12	b60	164	8	0.13	9124.93	0.4010	4.2	0.05457	1.4	0.053298	3.9	**343**	**5**	342	12	342	89	100
GP12	b44	493	25	0.06	16761.9	0.4017	2.4	0.05485	1.4	0.053109	2.0	**344**	**5**	343	7	333	45	103
GP12	b55	317	16	0.04	15968.4	0.4015	2.7	0.05487	2.0	0.05307	1.8	**344**	**7**	343	8	332	41	104
GP12	b41	367	21	0.60	3078.28	0.4041	4.9	0.05505	2.5	0.053246	4.2	**345**	**8**	345	14	339	95	102
GP12	b42	373	20	0.42	5439.11	0.4079	3.3	0.05506	1.8	0.053722	2.8	**346**	**6**	347	10	359	63	96
GP12	b46	1217	65	0.37	4048.2	0.4087	4	0.05508	1.7	0.053813	3.6	**346**	**6**	348	12	363	82	95
GP13	a29	543	30	0.51	3436.91	0.3924	4.2	0.05302	3.0	0.05367	3.0	**333**	**10**	336	12	357	68	93
GP13	a26	1349	77	0.62	5458.05	0.3929	3.5	0.05330	1.2	0.053465	3.3	**335**	**4**	337	10	349	75	96
GP13	a34	1728	105	0.93	1514.69	0.3875	5.1	0.05331	3.3	0.052725	3.9	**335**	**11**	333	15	317	89	106
GP13	a23	1609	82	0.11	3076.53	0.3902	3	0.05356	1.7	0.052847	2.4	**336**	**6**	335	9	322	56	104
GP13	a59	627	39	1.23	16558	0.3930	2.5	0.05388	1.8	0.052903	1.8	**338**	**6**	337	7	325	41	104
GP13	a48	747	49	1.19	513.606	0.3925	6.1	0.05392	2.1	0.052791	5.7	**339**	**7**	336	18	320	130	106
GP13	a31	732	39	0.26	1921.7	0.3972	5.7	0.05400	3.5	0.053345	4.5	**339**	**12**	340	17	343	103	99
GP13	a36	1634	84	0.16	5026.7	0.4028	3.1	0.05413	1.7	0.053961	2.6	**340**	**6**	344	9	369	58	92
GP13	a43	779	45	0.62	3494.11	0.3935	5.1	0.05414	2.0	0.052712	4.7	**340**	**7**	337	15	316	107	107

(*continued*)

TABLE 2. U-Pb ANALYTICAL DATA (*continued*)

Sample	Analysis	U (ppm)	Pb (ppm)	Th/U	$^{206}Pb/^{204}Pb$	$^{207}Pb/^{235}U$	2σ (%)	$^{206}Pb/^{238}U$	2σ (%)	$^{207}Pb/^{206}Pb$	2σ (%)	**$^{206}Pb/^{238}U$**	**2σ (Ma)**	$^{207}Pb/^{235}U$	2σ (Ma)	$^{207}Pb/^{206}Pb$	2σ (Ma)	Concordance (%)
GP13	a21	1898	102	0.27	5473.41	0.4028	3.6	0.05437	2.5	0.053727	2.5	**341**	**8**	344	10	360	57	95
GP13	a51	954	55	0.49	792.104	0.3960	4.2	0.05441	2.4	0.052784	3.5	**342**	**8**	339	12	320	79	107
GP13	a45	903	47	0.17	3877.71	0.4052	3.4	0.05445	2.3	0.053967	2.6	**342**	**8**	345	10	370	58	92
GP13	a54	296	16	0.14	1727.08	0.4015	7	0.05457	2.1	0.053365	6.7	**342**	**7**	343	21	344	152	99
GP13	a32	313	20	0.93	570.157	0.4037	9.6	0.05474	2.1	0.053485	9.3	**344**	**7**	344	28	349	211	98
GP13	a18	1724	98	0.56	8872.34	0.4027	2.9	0.05496	2.1	0.053146	2.0	**345**	**7**	344	8	335	46	103
GP13	a41	865	47	0.28	1101.4	0.4031	4.7	0.05497	1.9	0.053185	4.3	**345**	**6**	344	14	337	97	102
GP13	a55	342	19	0.42	5917.26	0.4013	6.7	0.05520	3.3	0.052719	5.8	**346**	**11**	343	20	317	132	109
GP13	a22	1908	101	0.15	1894.25	0.4056	3.4	0.05521	2.1	0.053285	2.6	**346**	**7**	346	10	341	60	102
GP13	a37	444	28	0.98	7511.99	0.4126	2.9	0.05526	1.6	0.054152	2.5	**347**	**5**	351	9	377	56	92
GP13	a28	1349	76	0.37	1065.99	0.4073	4.2	0.05564	2.9	0.053093	3.0	**349**	**10**	347	12	333	69	105
Inherited zircon																		
GP2	a12	200	20	0.15	203.06	0.7294	7.3	0.08904	1.2	0.059414	7.2	**550**	**7**	556	32	582	157	94
GP2	a10	95	17	1.09	122.667	1.1418	17	0.12612	1.4	0.065666	16.8	**766**	**10**	773	96	796	352	96
GP2	a5	149	25	0.63	1044.83	1.4925	4.3	0.15165	2.3	0.071383	3.7	**910**	**20**	927	27	968	75	94
GP2	a21	266	59	0.24	118.193	1.8341	5.2	0.17253	1.9	0.0771	4.8	**1026**	**18**	1058	35	1124	97	91
GP2	a27	66	15	0.64	207.855	1.8325	8.9	0.17624	1.6	0.075415	8.8	**1046**	**15**	1057	60	1080	176	97
GP2	a1	193	60	0.20	197.513	3.6256	4.5	0.26208	2.7	0.100331	3.6	**1500**	**36**	1555	36	1630	66	92
GP3	a42	56	4	0.22	2883.81	0.6252	6.9	0.07993	2.8	0.05673	6.3	**496**	**13**	493	27	481	139	103
GP4	a40	170	14	0.55	8146.75	0.6348	3.3	0.08020	1.4	0.057403	3.0	**497**	**7**	499	13	507	66	98
GP4	a23	209	105	0.48	4601.26	10.5904	1.8	0.45770	1.5	0.167814	1.1	**2429**	**30**	2488	17	2536	18	96
GP5	a39	58	5	0.80	2836.17	0.6030	5.5	0.07613	2.6	0.057451	4.8	**473**	**12**	479	21	509	105	93
GP5	a28	505	38	0.14	699.136	0.6074	4.7	0.07703	3.1	0.05719	3.6	**478**	**14**	482	18	499	79	96
GP5	a59	117	10	0.50	1720.69	0.6260	4.1	0.07820	3.2	0.058058	2.5	**485**	**15**	494	16	532	55	91
GP5	a60	26	2	0.43	2822.74	0.7034	5.6	0.08779	2.6	0.058109	4.9	**542**	**14**	541	24	534	108	102
GP5	a52	95	10	0.66	6468.03	0.7558	3.9	0.09162	2.3	0.059824	3.2	**565**	**12**	572	17	597	69	95
GP5	a56	26	3	0.91	1624.49	0.8096	4.6	0.09821	3.1	0.059788	3.5	**604**	**18**	602	21	596	75	101
GP6	a30	204	13	0.34	1756.1	0.4678	15	0.06269	2.4	0.054124	14.4	**392**	**9**	390	48	376	324	104
GP6	a31	222	15	0.46	5235.75	0.4876	4.5	0.06422	3.2	0.055073	3.2	**401**	**12**	403	15	415	71	97
GP6	a43	153	9	0.11	3177.8	0.4856	8.5	0.06422	3.2	0.054842	7.9	**401**	**12**	402	29	406	176	99
GP6	a22	80	6	0.31	2226.09	0.5905	6.2	0.07541	2.4	0.056791	5.7	**469**	**11**	471	24	483	127	97
GP6	a29	800	62	0.80	381.018	0.5935	4.6	0.07597	1.6	0.056662	4.3	**472**	**7**	473	17	478	95	99
GP6	a45	80	6	0.47	3610	0.5945	5.1	0.07599	2.8	0.056739	4.3	**472**	**13**	474	20	481	95	98
GP6	a33	131	12	0.97	3844.34	0.6050	5.5	0.07667	2.2	0.057236	5.1	**476**	**10**	480	21	501	111	95
GP6	a51	36	3	0.38	1722.24	0.6022	6.8	0.07667	3.5	0.056968	5.8	**476**	**16**	479	26	490	128	97
GP6	a11	247	18	0.11	7262.2	0.5974	3.4	0.07677	1.3	0.056435	3.1	**477**	**6**	476	13	470	70	102
GP6	a42	374	27	0.07	9980.24	0.6060	4.8	0.07703	3.8	0.057058	2.8	**478**	**18**	481	18	494	62	97
GP6	a15	318	23	0.08	7787.29	0.6089	3.8	0.07729	2.6	0.057144	2.8	**480**	**12**	483	15	497	61	97
GP6	a52	114	9	0.35	5571.88	0.6134	6.6	0.07754	4.0	0.057371	5.3	**481**	**19**	486	26	506	116	95
GP6	a56	96	7	0.36	5012.16	0.6067	3.3	0.07772	1.9	0.056613	2.7	**483**	**9**	481	13	476	59	101
GP6	a4	282	22	0.48	8682.53	0.6132	3	0.07784	1.1	0.057141	2.8	**483**	**5**	486	12	497	61	97
GP6	a54	89	6	0.10	1455.71	0.6077	4.2	0.07789	2.4	0.056584	3.5	**483**	**11**	482	16	475	77	102
GP6	a14	84	7	0.35	2420.08	0.6174	6.1	0.07832	3.0	0.057169	5.3	**486**	**14**	488	24	498	118	98
GP6	a60	61	5	0.52	1273.07	0.6187	9.4	0.07850	2.2	0.057163	9.2	**487**	**10**	489	37	498	202	98
GP6	a44	74	6	0.34	2964.09	0.6161	7.4	0.07859	2.7	0.056858	6.9	**488**	**13**	487	29	486	153	100
GP6	a13	79	6	0.19	2302.47	0.6092	5.8	0.07863	2.2	0.056187	5.4	**488**	**10**	483	22	460	119	106
GP6	a48	150	12	0.48	6490.8	0.6218	4.4	0.07893	1.5	0.057139	4.1	**490**	**7**	491	17	497	91	99
GP6	a20	178	13	0.14	4018.8	0.6117	4.7	0.07905	1.4	0.056124	4.4	**490**	**7**	485	18	457	99	107
GP6	a6	535	40	0.13	13683.7	0.6306	2.5	0.08022	1.3	0.05701	2.1	**497**	**6**	496	10	492	47	101
GP6	a10	520	46	0.29	17365.2	0.7263	2.7	0.08939	1.6	0.058922	2.2	**552**	**9**	554	12	564	47	98
GP6	a35	328	30	0.48	8073.86	0.7205	3.8	0.08950	2.0	0.058382	3.2	**553**	**11**	551	16	544	71	102
GP6	a32	220	23	0.91	4020.58	0.7336	5.4	0.09060	2.3	0.058731	4.9	**559**	**12**	559	23	557	106	100
GP6	a26	269	23	0.14	7296.94	0.7358	4.1	0.09087	1.9	0.058725	3.6	**561**	**10**	560	18	557	78	101
GP6	a9	237	22	0.24	6760.6	0.7704	3	0.09348	2.0	0.059775	2.3	**576**	**11**	580	13	595	49	97
GP6	a25	235	24	0.51	914.461	0.8185	4.7	0.09801	3.1	0.060566	3.6	**603**	**18**	607	22	624	78	97
GP6	a28	117	12	0.31	3916.6	0.8376	4	0.09912	2.1	0.061291	3.4	**609**	**12**	618	19	649	72	94
GP6	a53	17	2	1.36	1741.64	0.8360	7.9	0.10148	2.7	0.059747	7.4	**623**	**16**	617	37	594	160	105
GP6	a49	11	1	0.67	630.338	0.8473	13	0.10253	2.5	0.059936	13.2	**629**	**15**	623	64	601	285	105
GP6	a40	74	10	1.63	3216.09	0.8469	5.3	0.10277	2.3	0.05977	4.7	**631**	**14**	623	25	595	103	106
GP6	a41	228	23	0.30	5705.25	0.8638	4.7	0.10299	3.0	0.060828	3.6	**632**	**18**	632	22	633	79	100
GP6	a55	144	15	0.31	10452.8	0.9062	3.8	0.10547	2.5	0.062314	2.8	**646**	**16**	655	18	685	60	94
GP6	a19	129	17	1.56	4813.37	0.9027	4	0.10807	2.3	0.060583	3.3	**662**	**15**	653	20	624	71	106
GP6	a1	95	12	0.52	4357.16	1.0439	4.3	0.11816	2.0	0.064075	3.8	**720**	**13**	726	23	744	81	97
GP6	a8	161	21	0.40	3013.77	1.2031	3.2	0.13118	1.6	0.066515	2.8	**795**	**12**	802	18	823	59	97
GP6	a34	118	22	0.75	6485.97	1.7332	3.9	0.17448	1.4	0.072044	3.7	**1037**	**14**	1021	26	987	74	105

(*continued*)

TABLE 2. U-Pb ANALYTICAL DATA (*continued*)

Sample	Analysis	U (ppm)	Pb (ppm)	Th/U	$^{206}Pb/^{204}Pb$	$^{207}Pb/^{235}U$	2σ (%)	$^{206}Pb/^{238}U$	2σ (%)	$^{207}Pb/^{206}Pb$	2σ (%)	**$^{206}Pb/^{238}U$**	**2σ (Ma)**	$^{207}Pb/^{235}U$	2σ (Ma)	$^{207}Pb/^{206}Pb$	2σ (Ma)	Concordance (%)
GP6	a21	215	84	0.15	2971.83	7.2026	4.9	0.38836	2.9	0.13451	4.0	**2115**	**52**	2137	45	2158	69	98
GP6	a53	61	4	0.08	4254.79	0.6070	3.8	0.07756	2.0	0.056763	3.2	**482**	**9**	482	15	482	71	100
GP6	a51	33	3	0.32	2299.54	0.6996	5.5	0.08807	1.3	0.057611	5.3	**544**	**7**	539	23	515	117	106
GP6	a52	142	22	0.29	20771.5	1.5111	5.2	0.15238	4.3	0.071921	3.0	**914**	**37**	935	33	984	60	93
GP7	a25	77	6	0.72	2743.97	0.5873	4.6	0.07542	2.4	0.056471	3.9	**469**	**11**	469	17	471	87	100
GP7	a23	74	7	1.28	2609.38	0.5970	5.2	0.07591	1.9	0.05704	4.9	**472**	**9**	475	20	493	108	96
GP7	a39	44	4	1.16	1771.26	0.5905	7.3	0.07629	3.1	0.056141	6.6	**474**	**14**	471	28	458	147	103
GP7	a30	107	10	1.40	3815.57	0.6032	4.7	0.07665	2.5	0.057067	4.0	**476**	**11**	479	18	494	88	96
GP7	a7	69	6	0.95	680.194	0.5931	6.7	0.07666	2.8	0.056118	6.0	**476**	**13**	473	25	457	133	104
GP7	a26	149	14	1.40	5085.7	0.6098	4.6	0.07712	2.2	0.057354	4.0	**479**	**10**	483	18	505	88	95
GP7	a29	92	8	0.80	2636.34	0.6021	5.9	0.07715	2.2	0.056595	5.5	**479**	**10**	479	23	476	122	101
GP7	a14	61	5	0.94	2150.28	0.6051	6.5	0.07747	2.5	0.056648	6.0	**481**	**11**	480	25	478	133	101
GP7	a32	92	8	1.11	2986.44	0.6032	5.7	0.07749	1.8	0.056459	5.4	**481**	**8**	479	22	470	119	102
GP7	a6	66	6	0.94	1216.05	0.6170	4.6	0.07769	1.7	0.057603	4.3	**482**	**8**	488	18	515	94	94
GP7	a37	93	9	1.39	2152.79	0.6161	4.7	0.07775	2.2	0.057475	4.2	**483**	**10**	487	18	510	92	95
GP7	a1	104	10	1.35	4129.71	0.6047	4.9	0.07802	2.1	0.056217	4.5	**484**	**10**	480	19	461	99	105
GP7	a21	42	4	1.13	1221.29	0.6186	7.4	0.07842	2.4	0.057217	7.1	**487**	**11**	489	29	500	155	97
GP7	a5	39	4	1.22	1550.71	0.6243	7.8	0.07849	3.1	0.057692	7.1	**487**	**15**	493	31	518	156	94
GP7	a12	52	5	0.84	976.154	0.6156	6.3	0.07869	2.2	0.056744	5.9	**488**	**10**	487	25	482	130	101
GP7	a8	44	4	0.88	1721.74	0.6148	8	0.07889	2.4	0.056518	7.7	**490**	**11**	487	32	473	170	104
GP7	a18	57	5	1.18	2170.77	0.6167	6.1	0.07912	2.3	0.056534	5.6	**491**	**11**	488	24	473	124	104
GP7	a17	62	6	1.39	2312.68	0.6304	5.5	0.07957	1.8	0.057454	5.2	**494**	**9**	496	22	509	115	97
GP7	a38	270	20	0.10	2520.46	0.6325	3.1	0.07998	1.4	0.057358	2.7	**496**	**7**	498	12	505	60	98
GP7	a3	57	5	1.24	2192.82	0.6331	6.1	0.08055	2.5	0.057009	5.6	**499**	**12**	498	24	492	123	102
GP7	a10	48	5	0.93	2070.68	0.7215	5.4	0.08896	2.0	0.058827	5.0	**549**	**11**	552	23	561	108	98
GP7	a22	70	6	0.32	2591.5	0.7351	4.6	0.09024	2.4	0.059077	3.9	**557**	**13**	560	20	570	84	98
GP7	a9	35	4	1.33	1481.63	0.7383	8.7	0.09043	3.1	0.059213	8.1	**558**	**16**	561	38	575	177	97
GP7	a20	87	10	1.60	3107.25	0.7507	6.6	0.09247	2.4	0.058876	6.2	**570**	**13**	569	29	563	134	101
GP7	a19	78	8	0.80	3063.19	0.7637	4.8	0.09313	1.3	0.059476	4.7	**574**	**7**	576	22	585	101	98
GP8	a5	100	9	1.43	4182.85	0.6012	3.8	0.07659	1.8	0.056925	3.4	**476**	**8**	478	15	489	75	97
GP8	a8	56	5	1.48	678.534	0.6091	5	0.07792	2.0	0.056694	4.6	**484**	**9**	483	19	480	101	101
GP8	a39	95	9	1.70	2305.39	0.6312	3.9	0.07938	2.4	0.057672	3.1	**492**	**11**	497	15	517	68	95
GP8	a48	34	3	0.38	2067.08	0.6178	5.5	0.07962	1.9	0.056279	5.2	**494**	**9**	488	22	463	115	107
GP8	a49	170	14	1.10	3012.6	0.6323	6.8	0.07993	0.9	0.057372	6.7	**496**	**4**	498	27	506	148	98
GP8	a10	246	27	1.02	11598	0.8327	2.5	0.10016	1.2	0.060298	2.2	**615**	**7**	615	12	614	48	100
GP10	a36	1312	107	1.18	4231.32	0.6155	3.1	0.07929	1.3	0.056303	2.8	**492**	**6**	487	12	464	62	106
GP11	a25	392	36	0.41	4130.28	0.7344	3.2	0.08950	0.8	0.059516	3.1	**553**	**4**	559	14	586	68	94
GP11	a30	300	27	0.03	9554.59	0.8211	3.1	0.09903	1.3	0.060137	2.9	**609**	**7**	609	15	609	62	100
GP12	b59	391	26	0.61	4390.6	0.4674	2.2	0.06245	1.0	0.054282	2.0	**390**	**4**	389	7	383	45	102
GP13	a44	20	9	0.98	3168.4	6.3801	3.2	0.38738	1.9	0.119452	2.6	**2111**	**33**	2030	29	1948	47	108

If we compare the apparent age spectrum of inherited zircons in the ECS and the POS (Fig. 8C), it is noteworthy the POS peak age is late Ediacaran (ca. 550 Ma), interpreted as corresponding to zircons derived mainly from metaigneous rocks of the Cadomian arc and/or their erosion products (Fernández-Suárez et al., 1998, 2011). In contrast, the age peak of the inherited population in the ECS is ca. 485 Ma (Fig. 8C), an age corresponding to the voluminous magmatic event that took place in Iberia on the extended Gondwanan margin in Early Ordovician time, recorded in the Ollo de Sapo rocks (see Fig. 2).

The rocks related to the Ollo de Sapo event (dominated by rhyolites, ignimbrites, tuffs, and graywackes with high proportion of volcanic component; e.g., Díez-Montes, 2007) are strongly peraluminous. In contrast, Cadomian magmatism is metaluminous to weakly peraluminous (Fernández-Suárez et al., 1998; Rubio-Ordóñez et al., 2015). Therefore, the apparently more peraluminous nature of the ECS (cf. Fig. 5A) is consistent with the observation that the ECS granitoids might have recycled a higher proportion of the Ollo de Sapo protolith rocks than the POS granitoids, and likely also include a higher proportion of pelite component.

Another difference in the inheritance pattern between the ECS and the POS is the presence in the ECS of ca. 400–390 Ma zircon (Fig. 8C; see Introduction). This inherited component is also present in the syntectonic leucogranites (ca. 320 Ma; López-Moro et al., 2018) but absent in the POS. The origin of the zircons in this age group is not clear but zircons of this age are present in some mafic volcanic rocks in central Iberia (Gutiérrez-Alonso et al., 2008) and are also abundant as detrital components in Devonian–Carboniferous sequences of southwest Iberia, where they have been interpreted as derived from the dismantling of (intra?) Rheic oceanic arc rocks (Pereira et al., 2018).

Sample GP-12 (vaugnerite, Bayo-Vigo intrusion) contains the ca. 400–390 Ma inherited component (and apparently none of the others). This observation, pointing to some degree of crustal involvement, is consistent with the hypothesis of Scarrow et al. (2009), who argued that vaugnerites could represent magmas derived from a mantle metasome that intruded a crustal anatectic zone where some degree of mixing and mingling may take place.

Furthermore, and based on these observations, calculated zircon saturation temperatures (Table 1), and following the nomenclature of Miller et al. (2003), it can be considered that samples GP-2 and GP-7 represent

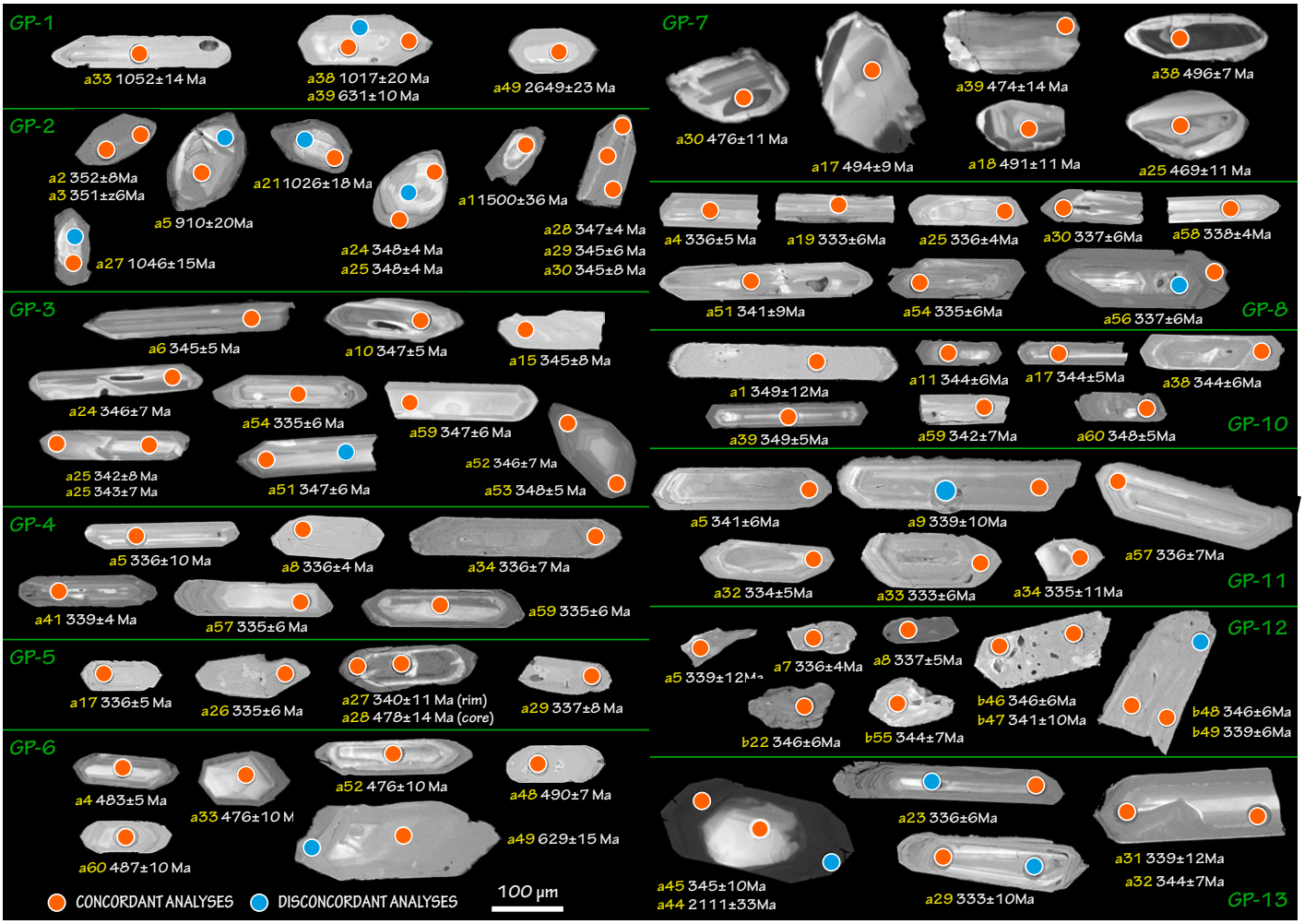

Figure 6. Representative cathodoluminescence images of the analyzed zircons. Orange spots mark the site of laser ablation–inductively coupled plasma–mass spectrometer U-Pb analyses with accompanying U-Pb age result. Blue spots mark the points where discordant analyses were obtained.

examples of cold granites because they display low Zr whole-rock contents (<150 ppm), low zircon saturation temperatures (<770 °C; Table 1) and high apparent inherited zircon content. Samples GP-3, GP-4, GP-10, and GP-11, at the opposite end, can be considered as hot granites displaying higher whole-rock Zr contents (>150 ppm), higher zircon saturation temperatures (>780 °C), and low apparent inheritance (<5%). Sample GP-6A (Zr content 150 ppm; zircon saturation temperature ~815 °C; moderate inheritance ~20%) and sample GP-8 (Zr content 142 ppm; zircon saturation temperature ~776 °C; moderate apparent inheritance ~17%) are between clear-cut hot or cold granites.

Sample GP-12 (vaugnerite) with very low apparent inheritance (<3%) has a low zircon saturation temperature, ~764 °C (Table 1), which in this case probably suggests undersaturation of Zr in the source (cf. Miller et al., 2003).

The zircon saturation temperatures of the ECS granitoids, based on our analyses and those available in the literature (Fig. 9A), have a bimodal distribution with maxima ~803 °C and 704 °C, essentially corresponding to the apparent occurrence in the suite of hot and cold granitoids (sensu Miller et al., 2003) with an apparent predominance of the former. This is consistent with the Ba and Pb contents and Pb/Ba ratios of these granitoids (Table 1; Fig. 9B). On the diagram of Finger and Schiller (2012) they plot on both sides of the empirical line that separates primary lower temperature S-type (muscovite ± incipient biotite breakdown) and higher temperature S-types (muscovite + biotite breakdown), which represent the predominant type in our data set in agreement with the apparent predominance of hot granites.

In our case study there seems to be little or no correlation between the inheritance features and other geochemical parameters (e.g., ASI, SiO_2 content, maficity) or crystallization age within the suite, in agreement with the observations made by Miller et al. (2003).

DISCUSSION

The primary conclusion of this study is that it proves the existence of a volumetrically significant Visean magmatic event in northwest Iberia. Except for sample GP-1, the age of which remains unconstrained, the age data of all other samples in this study confirm the existence of an early granodiorite group between 347 and 337 Ma, as assumed by previous work. Therefore, the ECS constitutes the oldest known manifestation of Variscan magmatism in northwest Iberia.

The first objective of this study has been fulfilled and our results challenge any model, hypothesis, or speculation that does not take this evidence into account.

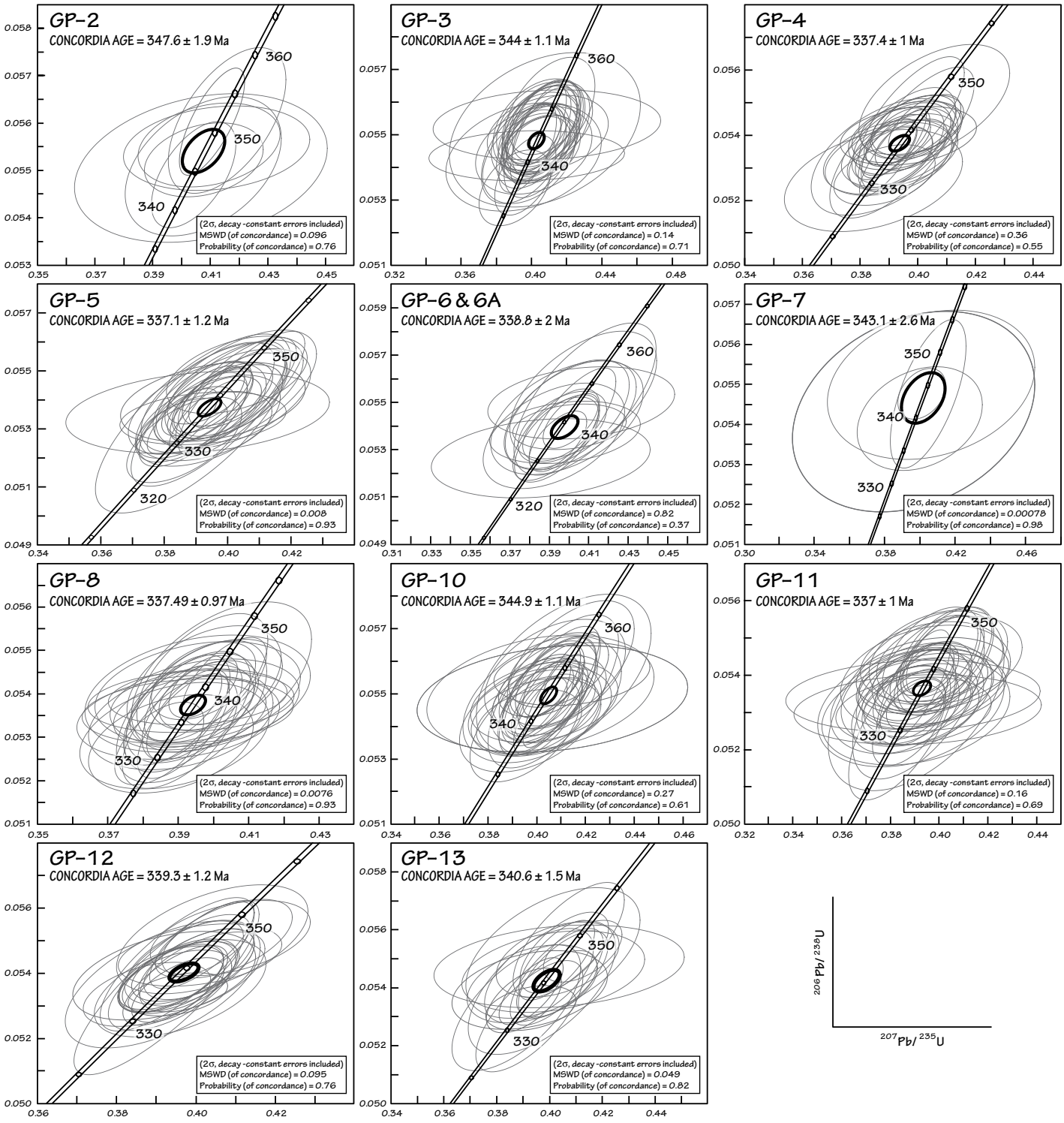

Figure 7. Wetherill concordia diagrams showing the calculated concordia age, error, and mean square of weighted deviates (MSWD) for each of the studied samples. These ages are interpreted to represent the best estimate for the crystallization age of the corresponding intrusion (see text for details).

TABLE 3. SAMPLE LOCATION, INTRUSION AGES, AND INHERITED ZIRCON AGES FOR EACH OF THE STUDIED SAMPLES

Sample	Pluton	Coordinates (°N, °W)	Concordant analyses (%)	Analyses used in the concordia diagrams	Age and error (Ma, 2σ)	Concordant inherited zircon ages (older than 350 Ma) (number, %)	Inherited zircon ages (Ma)
GP-2	Ricobayo	41.526552, 6.021074	41	8	347.6 ± 1.9	6 (43%)	1500–550
GP-3	Palas de Rei	42.613733, 7.756814	54	34	344.0 ± 1.1	1	496
GP-4	Palas de Rei	42.872540, 7.880200	48	28	337.4 ± 1.0	2	2500–497
GP-5	Espenuca (Betanzos)	43.380850, 8.132559	60	31	337.4 ± 1.2	6 (17%)	604–473
GP-6 , GP-6A	Espenuca (Irixoa)	43.284738, 8.051695	61	17	338.8 ± 2.0	42 (70%)	2100–392
GP-7	Espenuca (Pontedeume)	43.221899, 8.106465	50	5	343.1 ± 2.6	25 (80%)	574–470
GP-8	Santa Comba–Negreira	43.053348, 8.765807	56	30	337.5 ± 1.0	6 (17%)	615–476
GP-10	Meabia	42.658030, 8.378344	56	35	344.9 ± 1.1	1	492
GP-11	Bayo-Vigo	42.259074, 8.765712	68	41	337.0 ± 1.0	2	609–553
GP-12	Bayo-Vigo (vaugnerite)	42.263086, 8.756089	49	28	339.3 ± 1.2	1	390
GP-13	Avión	42.379507, 8.254504	33	20	340.6 ± 1.5	1	2100

Moreover, our study has not included all intrusions that are possible candidates to belong to the ECS in northwest Iberia. Accordingly, it is to be expected that further geochronological work will reveal the existence of more intrusions in this age bracket in the northwest Iberian realm of the WEVB (e.g., northern Portugal, southeast CIZ). In addition, the syntectonic leucogranitoids generated ca. 320 Ma and the POS contain abundant ca. 340 Ma inherited zircon (Martín Garro, 2015; López-Moro et al., 2018), even in areas without any known exposures of the ECS granitoids. This is another argument in favor of the idea that the ECS represents a larger than hitherto considered magmatic event in northwest Iberia.

As reported here, the ages of the dated intrusions range between ca. 347 and 337 Ma. These ages suggest that the magmatic event that produced this suite of Visean granitoids in northwest Iberia was relatively short lived (ca. 10 Ma) when compared with the time span of the POS in the same geological realm (ca. 310–287 Ma, a duration of >20 m.y.; Gutiérrez-Alonso et al., 2011, and references therein).

What we consider geologically relevant based on our data is that, in devising a geodynamic scenario for the genesis of the ECS in northwest Iberia, it may be worth pursuing the notion that this event was short lived and voluminous (see Fig. 2) and thus could be considered as a sort of magmatic flare-up.

Another relevant datum issuing from this work is the age of the vaugnerite rocks in the Bayo-Vigo intrusion, which is coeval with many vaugnerite and/or durbachite rocks in the Variscan realm of western Europe (e.g., von Raumer et al., 2014). This is important because there are also younger vaugnerite and/or durbachite rocks in the Variscan realm (e.g., Moyen et al., 2017) that would be linked to different petrogenetic-geodynamic scenarios. In this regard, note that in Fernández-Suárez et al. (2000) it was shown that hornblende-bearing peridotites (known as in the regional literature as cortlandites) spatially associated with the ca. 325 Ma Vivero granitoid intrusion (also in the northwest Iberian realm) represent a later event of mantle melting ca. 290 Ma.

Essentially, the ages of sample GP-12 proves that there are mantle-derived rocks associated and coeval with the ECS of granitoids, and that they are linked to their petrogenetic-geodynamic scenarios.

The ages obtained for the vaugnerite (sample GP-12; 339 ± 1 Ma) and the main granodiorite facies (sample GP-11; 337 ± 1 Ma) of the Bayo-Vigo intrusion (Fig. 2) overlap within error, albeit the mafic rocks yield a concordia age ~2 m.y. older than the granodiorites. These ages indicate that although essentially coeval, the crystallization of mafic magmas took place slightly earlier than that of the main granodiorite unit. This observation points to a slight age difference in the spatially related mafic and granite rocks and is consistent with Gallastegui's (2005) interpretation (based on field, mineralogical, geochemical, and isotope data) that the mafic and granitoid magmas, although physically mingled, had essentially separate chemical evolutions. This is also in agreement with some of the current views on the origin of the chemical diversity in granitoids that place little emphasis on actual magma mixing as a source of chemical variation (e.g., Clemens and Stevens, 2012).

Based on the information reported, and on previous studies in the area, a hypothesis for the generation of the ECS of northwest Iberia needs to consider the following.

1. The ECS of northwest Iberia represents an apparently short lived event with generation of a significant volume of granitoid magma in a relatively short period of time (~5–10 m.y.). It is convenient to highlight here that the apparent short duration of the ECS event contrasts with the longer time span of the POS in the same northwest Iberian realm in which there seems to have been a protracted time span of granitoid production between ca. 310 and 287 Ma (although mostly between 305 and 290; Gutiérrez-Alonso et al., 2011).

2. The Visean magmatic event reported herein generated mainly peraluminous crustal granitoids that recycled mostly the early Paleozoic and late Ediacaran basement rocks of northwest Iberia. Melt temperatures were ~700 to >800 °C with an apparent predominance of hot granitoids generated through melting processes that likely involved muscovite and muscovite + biotite breakdown reactions. In the intrusion of Bayo-Vigo, where we have proven the coeval nature of vaugnerites and granitoids, the main granite facies is a hot granitoid (sample GP-11). It is remarkable that ash-fall beds in the Carboniferous strata of the neighboring Cantabrian zone of northwest Iberia dated as ca. 340 Ma (Merino Tomé et al., 2017) indicate that this event also produced volcanic activity, the magnitude of which it is not possible to constrain with available geological evidence, in particular owing to the poor preservation of Visean sedimentary rocks throughout the CIZ.

3. There is some involvement of mantle melting, as attested to by the presence of coeval vaugnerite rocks.

Based on these three points, we must invoke a geodynamic scenario compatible with relatively fast production of significant amounts of crustal granitoid melts and coeval production of minor melts extracted from the underlying subcontinental lithospheric mantle in the broader scenario of the Variscan collision in the northwest Iberian Variscan realm.

It is also important to note that these granitoids appear as elongate intrusions that follow the structural grain of the emplacement region and appear to be absent in the most external parts of the orogen (West Asturian Leonese and Cantabrian zones; Figs. 1 and 2), at variance with the POS that is present across the entire orogen, including the foreland fold and thrust belt (Cuesta and Gallastegui, 2007; Gutiérrez-Alonso et al., 2011).

Several models involving varied and contrasting geodynamic scenarios have been proposed to explain the origin of early Carboniferous

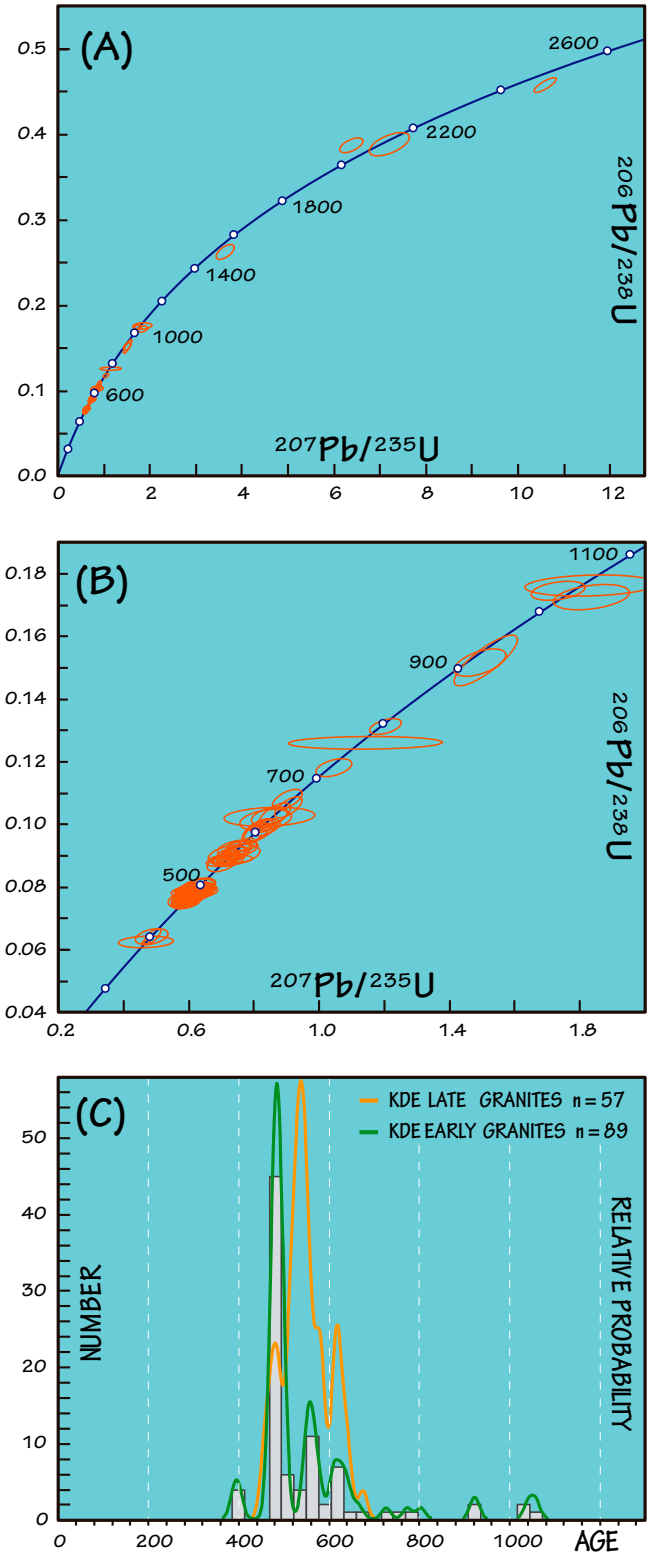

Figure 8. U-Pb ages of inherited zircon in the studied samples. (A) Concordia plot showing all inherited zircon concordant analyses. (B) Concordia plot showing inherited zircons younger than ca. 1 Ga. (C) Plot showing the histogram and KDE (kernel density estimation) for the U-Pb ages of inherited zircon in the early Carboniferous suite. For comparison (see text) we have added the KDE of U-Pb ages of inherited zircon in the postorogenic granitoid suite granitoids.

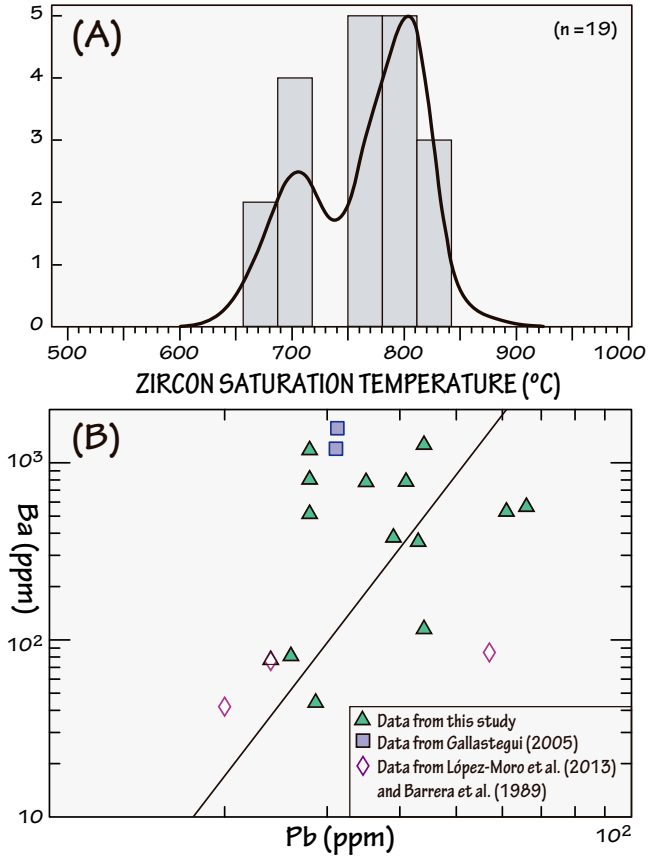

Figure 9. (A) KDE (kernel density estimation) plot of the zircon saturation temperature (calculated according to Watson and Harrison, 1983) for the early Carboniferous suite (ECS) granitoids (see main text for details). (B) Pb versus Ba diagram (Finger and Schiller, 2012) for the ECS granitoids (see main text for details).

magmatism in the European Variscan Belt. We argue that these models are difficult to extrapolate to the northwest Iberian Variscan realm, as they cannot be easily reconciled with available geological observations in the region.

Models invoked to explain the origin of this magmatic event in the Variscan Belt include: (1) persistent subduction under the Gondwanan margin until ca. 340 Ma (Janoušek and Holub, 2007); (2) slab break-off of the southward-directed subduction of the Rheic oceanic crust (e.g., Kubínová et al., 2017); (3) mantle wedge metasomatism (Finger et al., 2007); (4) late collisional slab sinking and subduction inversion (von Raumer et al., 2014); (5) relamination, rheological weakening, and radiogenic heat (Schulmann et al., 2014); and (6) strike-slip wrenching (Edel, 2001; Rossi et al., 2009).

All of these models except 5 have in common that magmatism is thought to have occurred in the upper plate, which is a primary inconsistency with geological data available for the northwest Iberian realm, which indicate that all the granitoids dated in this work intruded in the lower plate (Fig. 10; see following).

Most models proposed for the Variscan evolution of northwest Iberia (e.g., Martínez Catalán et al., 2002, 2007; Ribeiro et al., 2007; Gómez Barreiro et al., 2010; Pastor-Galán et al., 2013; Díez Fernández et al., 2016) agree that the continental margin of Gondwana underwent westward (in present-day coordinates) directed subduction down to ~80 km (26 kbar in eclogites; Rodríguez et al., 2003; 22 kbar in blueschists; López-Carmona et al., 2013, 2014) at 370–360 Ma (Rodríguez et al., 2003; Abati et al., 2010; López-Carmona et al., 2014; Fig. 10A). Subduction

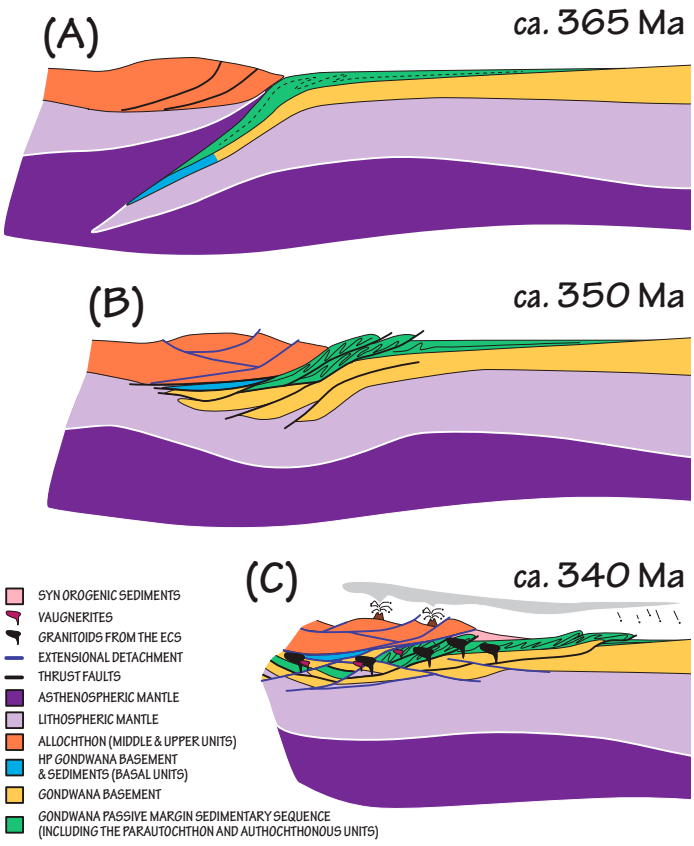

Figure 10. Model depicting our favored hypothesis to explain the genesis of the early Carboniferous suite (ECS). HP—high pressure. (A) Reconstruction ca. 365 Ma (Martínez Catalán et al., 2007; López-Carmona et al., 2014, and references therein) when the Gondwanan passive margin acted as the lower plate and was subducted down to a depth of ~70 km. (B) Exhumation due to buoyancy, extension in the upper plate (allochthonous complexes) and generation of a lithospheric thickened root under the complexes, involving some lithospheric mantle wedges ca. 350 Ma. Deformation in the parautochthon and autochthonous units advances toward the east (in present-day coordinates). (C) Extension of the thickened crust accompanied by crustal melting and sparse lithospheric mantle melting. Magmatic intrusions caused also volcanic activity in the surface; ash-fall deposits are recorded in the foreland of the orogen, where deformation had not yet started.

was followed by the exhumation of the subducted Gondwanan rocks that were subsequently overthrust onto what is currently known as the parautochthon and autochthon domains (Fig. 10B). Exhumation took place ca. 360–350 Ma (Santos Zalduegui, 1995; Rodríguez et al., 2003; López-Carmona et al., 2014), and final emplacement of the allochthonous units happened through an out-of-sequence thrusting event ca. 350–340 Ma (Dallmeyer et al., 1997; Martínez Catalán et al., 1996, 2002; Gómez Barreiro et al., 2006, 2010; López-Carmona et al., 2014). The emplacement of the allochthonous units was coeval with widespread recumbent folding and a subsequent thrusting event in the internal zones of the autochthonous units (Rubio Pascual, 2013; Martínez-Catalán et al., 2014). Given that the studied granitoids mostly intrude the parautochthonous unit around the allochthonous complexes (Fig. 2), it is important to keep in mind the above information in order to propose a tentative scenario for the generation of the ECS in northwest Iberia.

Figure 10 illustrates our favored hypothesis for the genesis of the ESC of Iberia and endeavors to take into account the observations presented here, as well as the general framework of the geodynamic scenarios of the Variscan collision in northwest Iberia.

Our starting point is the widely agreed upon scenario in which the most seaward part of the Gondwanan continental platform was overridden by another continental block (generally considered to have been Laurussia). The Gondwanan lower plate was subducted to a depth of ~70 km (ca. 370–360 Ma; Fig. 10A, see preceding references) before starting its exhumation path. The exhumation of this portion of the subducted Gondwanan passive margin caused its overthrusting onto the Paleozoic sedimentary sequence located in the non-subducted Gondwanan realms (i.e., the parautochthonous and autochthonous CIZ units; Figs. 1 and 2).

Exhumation of the subducted units was accompanied by shortening in the parautochthonous and autochthonous units, recorded as recumbent folding in the overthrusted sedimentary sequence ca. 360–350 Ma (Dallmeyer et al., 1997; Fig. 10B). Together with the superposition of the allochthonous complexes onto the parautochthonous and autochthonous units, the shortening also led to crustal duplexing at lower levels, causing the duplication of the crust and substantial increase in crustal and lithospheric mantle thickness and arguably some lithospheric mantle wedging (Fig. 10B).

Alternating episodes of shortening and extension happened subsequently as deformation progressed toward the foreland (Dallmeyer et al., 1997; Martínez Catalan et al., 2007; Gómez-Barreiro et al., 2006; Rubio-Pascual et al., 2013; Díez-Fernández et al., 2016). The earliest extensional events are likely to have occurred after the initial thickening in the lower plate and to have been localized in domains where maximum thickness was attained under the allochthonous and parautochthonous units (Fig. 10C).

In our interpretation, the presence of this thickened crust (~70 km) may have been ultimately responsible for the extension that in turn triggered crustal (and minor mantle) melting. Melts thus produced would have migrated upward until their final emplacement at mid-crustal levels, although some of these melts were erupted and preserved as ash-fall deposits (Merino-Tomé et al., 2017) (Fig. 10C). Crustal melts would have formed the granitoid intrusions that we studied and the minor vaugneritic bodies could have been generated by melting of the lithospheric mantle when some of the mantle wedges mentioned herein were decompressed upon exhumation. In this context we tentatively envisage a pattern whereby the higher temperature granitoids might have been generated in melting loci where the mantle was involved (providing extra heat upon melting) and the cold granitoids generated in melting loci where only crust was involved. Exhumation happened at a fast rate (2.0–2.5 cm/yr) consistent with the apparent short time span of granitoid production that our geochronological data suggest (López-Carmona et al., 2014). Therefore, we argue that fast exhumation of a thickened and fertile crust (and some wedged-in lithospheric mantle) led to rapid melt production (magmatic flare-up) that seems to have ended ca. 337 Ma.

Subsequent shortening ca. 335–325 Ma resulted in a rethickening of the crust, followed by extension and the generation of the metamorphic domes (Martínez Catalán et al., 2014, and references therein) where the studied rocks are currently exposed, surrounded in some cases by a younger generation of crustal leucogranitoids formed ca. 320 Ma (López-Moro et al., 2017; Díez-Fernández et al., 2017). The presence of abundant ca. 340 Ma zircon xenocrysts in the younger leucogranitoids (e.g., Martín Garro, 2015; López-Moro et al., 2018) indicate that the ECS granitoids were involved (i.e., acted as protolith rocks) in the generation of the syn-extensional leucogranitoids ca. 320 Ma.

CONCLUSIONS

The geochronological work carried out in this study proves that the so-called early granodiorites in northwest Iberia represent a distinct,

short-lived, relatively voluminous magmatic event that took place in Visean time, between ca. 347 and 337 Ma.

This magmatic event produced mainly crustal peraluminous granitoids with minor associated mafic rocks and volcanics.

The hypothesis proposed to explain the genesis of this early Carboniferous magmatic event in the context of the Variscan collision in the WEVB involves subduction of the Gondwanan crust under Laurussia or another Gondwanan element followed by rapid exhumation of the thickened crust. Fast exhumation led to rapid melt production and a relatively short lived magmatic event (flare-up) recorded in the ECS granitoids that we studied.

The existence of this Visean magmatic event explains the abundance of ca. 340 Ma zircon xenocrysts in younger granitoids of northwest Iberia, leading to the interpretation that the ECS granitoids acted as a source rock in subsequent Variscan crustal melting episodes.

ACKNOWLEDGMENTS

This work has been funded by the Spanish Ministry of Economy and Competitiveness under the project ODRE III—Oroclines & Delamination: Relations & Effects (CGL2013-46061-P) and Происхождение, металлогения, климатические эффекты и цикличность Крупных Изверженных Провинций (КИП) (Origin, metallogeny, climatic effects, and cyclical large igneous provinces) (14.Y26.31.0012; Russian Federation) to Gutiérrez-Alonso and López-Carmona and CGL-2016-76438-P to Fernández-Suárez. López-Carmona was also funded by a "Juan de la Cierva" grant (reference FJCI-2014-20740). Assistance by M. Hofmann, U. Linnemann, and R. Krause at the Senckenberg Naturhistorische Sammlungen Dresden is greatly appreciated. We thank Elena Núñez Guerrero for assistance in zircon processing and X. Arroyo for his help with cathodoluminescence imaging. This paper is part of UNESCO IGCP (United Nations Educational, Scientific and Cultural Organization International Geoscience Programme) Project 574: Buckling and Bent Orogens, and Continental Ribbons; Project 597: Amalgamation and Breakup of Pangaea: The Type Example of the Supercontinent Cycle; and Project 648: Supercontinent Cycles & Global Geodynamics. We thank the editor and two anonymous reviewers for their constructive reviews.

REFERENCES CITED

Abati, J., and Dunning, G.R., 2002, Edad U-Pb en monacitas y rutilos de los paragneises de la Unidad de Agualada (Complejo de Ordenes, NW del Macizo Ibérico): Geogaceta, v. 32, p. 95–98.

Abati, J., Gerdes, A., Fernández-Suárez, J., Arenas, R., Whitehouse, M.J., and Fernández, R.D., 2010, Magmatism and early Variscan continental subduction in the northern Gondwana margin recorded in zircons from the Basal Units of Galicia, NW Spain: Geological Society of America Bulletin, v. 122, p. 219–235, https://doi.org/10.1130/B26572.1.

Alcock, J.E., Martínez Catalán, J.R., Rubio Pascual, F.J., Díez Montes, A., Díez Fernández, R.D., Gómez Barreiro, J., Arenas, R., da Silva, Í.D., and González Clavijo, E., 2015, 2-D thermal modeling of HT–LP metamorphism in NW and Central Iberia: Implications for Variscan magmatism, rheology of the lithosphere and orogenic evolution: Tectonophysics, v. 657, p. 21–37, https://doi.org/10.1016/j.tecto.2015.05.022.

Arenas, R., et al., 2016, Allochthonous terranes involved in the Variscan suture of NW Iberia: A review of their origin and tectonothermal evolution: Earth-Science Reviews, v. 161, p. 140–178, https://doi.org/10.1016/j.earscirev.2016.08.010.

Ballèvre, M., Bosse, V., Ducassou, C., and Pitra, P., 2009, Palaeozoic history of the Armorican Massif: Models for the tectonic evolution of the suture zones: Comptes Rendus Geoscience, v. 341, p. 174–201, https://doi.org/10.1016/j.crte.2008.11.009.

Ballèvre, M., et al., 2014, Correlation of the nappe stack in the Ibero-Armorican arc across the Bay of Biscay: A joint French-Spanish project, *in* Schulmann, K., et al., eds., The Variscan orogeny: Extent, timescale and the formation of the European crust: Geological Society of London Special Publication 405, p. 77–113, https://doi.org/10.1144/SP405.13

Barrera, J.L., Farias, P., González Lodeiro, F., Marquínez, J., Martín Parra, L.M., Martínez Catalán, J.R., Olmo Saenz, A., and De Pablo Maciá, J.G., 1989, Hoja y Memoria del Mapa Geológico Nacional E 1:200.000 n° 17 (Orense-Verín): Madrid, Instituto Geológico y Minero de España, 284 p.

Bea, F., 2012, The sources of energy for crustal melting and the geochemistry of heat-producing elements: Lithos, v. 153, p. 278–291, https://doi.org/10.1016/j.lithos.2012.01.017.

Bea, F., Montero, P., and Molina, J.F., 1999, Mafic precursors, peraluminous granitoids, and late lamprophyres in the Avila batholith: A model for the generation of Variscan batholiths in Iberia: Journal of Geology, v. 107, p. 399–419, https://doi.org/10.1086/314356.

Bea, F., Montero, P.G., González-Lodeiro, F., Talavera, C., Molina, J.F., Scarrow, J.H., Whitehouse, M.J., and Zinger, T., 2006a, Zircon thermometry and U-Pb ion-microprobe dating of the gabbros and associated migmatites of the Variscan Toledo Anatectic Complex, Central Iberia: Journal of the Geological Society [London], v. 163, p. 847–855, https://doi.org/10.1144/0016-76492005-143.

Bea, F., Montero, P., Talavera, C., and Zinger, T., 2006b, A revised Ordovician age for the Miranda do Douro orthogneiss, Portugal: Zircon U-Pb ion-microprobe and LA-ICPMS dating: Geologica Acta, v. 4, p. 395–401.

Bea, F., Montero, P., and Zinger, T., 2003, The nature, origin, and thermal influence of the granite source layer of Central Iberia: Journal of Geology, v. 111, p. 579–595, https://doi.org/10.1086/376767.

Bellido Mulas, F., González Lodeiro, F., Klein, E., Martínez Catalán, J.R., and Pablo Maciá, J.G., 1987, Las rocas graníticas del norte de Galicia y occidente de Asturias: Memoria del Instituto Geológico y Minero de España, v. 101, 157 p.

Braid, J.A., Murphy, J.B., Quesada, C., Bickerton, L., and Mortensen, J.K., 2012, Probing the composition of unexposed basement, South Portuguese Zone, southern Iberia: Implications for the connections between the Appalachian and Variscan orogens: Canadian Journal of Earth Sciences, v. 49, p. 591–613, https://doi.org/10.1139/e11-071.

Buda, G., Koller, F., and Ulrych, J., 2004, Petrochemistry of Variscan granitoids of Central Europe: correlation of Variscan granitoids of the Tisia and Pelsonia Terranes with granitoids of the Moldanubicum, Western Carpathian and Southern Alps. A review: Part I: Acta Geologica Hungarica, v. 47, p. 117–138, https://doi.org/10.1556/AGeol.47.2004.2-3.3.

Cambeses, A., Scarrow, J.H., Montero, P., Molina, J.F., and Moreno, J.A., 2015, SHRIMP U-Pb zircon dating of the Valencia del Ventoso plutonic complex, Ossa-Morena Zone, SW Iberia: Early Carboniferous intra-orogenic extension-related 'calc-alkaline'magmatism: Gondwana Research, v. 28, p. 735–756, https://doi.org/10.1016/j.gr.2014.05.013.

Capdevila, R., 1969, Le metamorphisme regional progressif et les granites dans le segment Hercynien de Galice Nord Orientale (NW de L'Espagne) [Ph.D. thesis]: Montpellier, France, Université de Montpellier, 430 p.

Capdevila, R., and Floor, P., 1970, Les différents types de granites hercyniens et leur distribution dans le nord ouest de l'Espagne: Boletín Geológico y Minero, v. LXXXI, p. 215–225.

Capdevila, R., Corretge, G., and Floor, P., 1973, Les granitoides varisques de la Meseta Ibérique: Bulletin de la Société Géologique de France, v. 7, no. 3–4, p. 209–228, https://doi.org/10.2113/gssgfbull.S7-XV.3-4.209.

Cartannaz, C., Rolin, P., Cocherie, A., Marquer, D., Legendre, O., Fanning, C.M., and Rossi, P., 2007, Characterization of wrench tectonics from dating of syn- to post-magmatism in the north-western French Massif Central: International Journal of Earth Sciences, v. 96, p. 271–287, https://doi.org/10.1007/s00531-006-0101-y.

Castro, A., Patiño Douce, A.E., Corretgé, L.G., De La Rosa, J.D., El-Biad, M., and El-Hmidi, H., 1999, Origin of peraluminous granites and granodiorites, Iberian massif, Spain: An experimental test of granite petrogenesis: Contributions to Mineralogy and Petrology, v. 135, p. 255–276, https://doi.org/10.1007/s004100050511.

Castro, A., Corretgé, L.G., El-Biad, M., El-Hmidi, H., Fernández, C., and Patiño Douce, A.E., 2000, Experimental constraints on Hercynian anatexis in the Iberian Massif, Spain: Journal of Petrology, v. 41, p. 1471–1488, https://doi.org/10.1093/petrology/41.10.1471.

Clemens, J.D., 2014, Element concentrations in granitic magmas: Ghosts of textures past?: Journal of the Geological Society [London], v. 171, p. 13–19, https://doi.org/10.1144/jgs2013-008.

Clemens, J.D., and Stevens, G., 2012, What controls chemical variation in granitic magmas?: Lithos, v. 134, p. 317–329, https://doi.org/10.1016/j.lithos.2012.01.001.

Cuesta, A., and Gallastegui, G., 2007, El magmatismo varisco postcinemático en zonas externas del NO del Macizo Ibérico: XV Semana-VI Congreso Ibérico de Geoquímica, p. 11–16 (DVD-ROM).

Da Silva, Í.D., Linnemann, U., Hofmann, M., González Clavijo, E., Díez Montes, A., and Martínez Catalán, J.R., 2015, Detrital zircon and tectonostratigraphy of the Parautochthon under the Morais Complex (NE Portugal): Implications for the Variscan accretionary history of the Iberian Massif: Journal of the Geological Society [London], v. 172, p. 45–61, https://doi.org/10.1144/jgs2014-005.

Dallmeyer, R.D., and Gil Ibarguchi, J.I., 1990, Age of amphibolitic metamorphism in the ophiolitic unit of the Morais allochthon (Portugal): Implications for early Hercynian orogenesis in the Iberian Massif: Journal of the Geological Society [London], v. 147, p. 873–878, https://doi.org/10.1144/gsjgs.147.5.0873.

Dallmeyer, R.D., García-Casquero, J.L., and Quesada, C., 1995, $^{40}Ar/^{39}Ar$ mineral age constraints on the emplacement of the Burguillos del Cerro igneous complex (Ossa-Morena zone, SW Iberia): Boletín Geológico y Minero, v. 106, p. 3–14.

Dallmeyer, R.D., Martínez-Catalán, J.R., Arenas, R., Gil Ibarguchi, J.I., Gutiérrez-Alonso, G., Farias, P., Bastida, F., and Aller, J., 1997, Diachronous Variscan tectonothermal activity in the NW Iberian Massif: Evidence from $^{40}Ar/^{39}Ar$ dating of regional fabrics: Tectonophysics, v. 277, p. 307–337, https://doi.org/10.1016/S0040-1951(97)00035-8.

Den Tex, E., 1966, Apercu petrologique et structural de la Galice cristalline: Leidse Geologische Mededelingen, v. 36, p. 211–223.

De Pablo Maciá, P., 1981, Contribución a la correlación y síntesis de los granitos gallegos: Cadernos do Laboratotio Xeolóxico de Laxe, v. 2, p. 51–60.

Dias, G., Leterrier, J., Mendes, A., Simoes, P.P., and Bertrand, J.M., 1998, U-Pb zircon and monazite geochronology of post-collisional Hercynian granitoids from the Central Iberian Zone (Northern Portugal): Lithos, v. 45, p. 349–369, https://doi.org/10.1016/S0024-4937(98)00039-5.

Díaz Alvarado, J., Fernández, C., Castro, A., and Moreno-Ventas, I., 2013, SHRIMP U-Pb zircon geochronology and thermal modeling of multilayer granitoid intrusions: Implications for the building and thermal evolution of the Central System batholith, Iberian Massif, Spain: Lithos, v. 175, p. 104–123, https://doi.org/10.1016/j.lithos.2013.05.006.

Díez Fernández, R., and Pereira, M.F., 2016, Extensional orogenic collapse captured by strike-slip tectonics: Constraints from structural geology and U-Pb geochronology of the Pinhel shear zone (Variscan orogen, Iberian Massif): Tectonophysics, v. 691, p. 290–310, https://doi.org/10.1016/j.tecto.2016.10.023.

Díez Fernández, R., Arenas, R., Pereira, M.F., Sánchez-Martínez, S., Albert, R., Martín Parra, L.M., Rubio Pascual, F.J., and Matas, J., 2016, Tectonic evolution of Variscan Iberia: Gondwana-Laurussia collision revisited: Earth-Science Reviews, v. 162, p. 269–292, https://doi.org/10.1016/j.earscirev.2016.08.002.

Díez Fernández, R., Martín Parra, L.M., and Rubio Pascual, F.J., 2017, Extensional flow produces recumbent folds in syn-orogenic granitoids (Padrón migmatitic dome, NW Iberian Massif): Tectonophysics, v. 703, p. 69–84, https://doi.org/10.1016/j.tecto.2017.03.010.

Díez Montes, A., 2007, La Geología del Dominio Ollo de Sapo en las comarcas de Sanabria y Terra do Bolo: Serie Nova Terra 34: Área de Xeoloxía e Minería do Seminario de Estudos Galegos, A Coruña, 494 p.

Díez Montes, A., Martínez Catalán, J.R., and Bellido Mulas, F., 2010, Role of the Ollo de Sapo massive felsic volcanism of NW Iberia in the Early Ordovician dynamics of northern Gondwana: Gondwana Research, v. 17, p. 363–376, https://doi.org/10.1016/j.gr.2009.09.001.

Dupuis, N.E., Braid, J.A., Murphy, J.B., Quesada, C., and McFarlane, C., 2014, Changing mantle sources in a suture zone in the heart of Pangea: Implications for collisional tectonics during the waning stages of ocean closure: International Journal of Earth Sciences, v. 103, p. 1403–1414, https://doi.org/10.1007/s00531-014-1012-y.

Edel, J.B., 2001, The rotations of the Variscides during the Carboniferous collision: Paleomagnetic constraints from the Vosges and the Massif Central (France): Tectonophysics, v. 332, p. 69–92, https://doi.org/10.1016/S0040-1951(00)00250-X.

Eichhorn, R., Loth, G., Höll, R., Finger, F., Schermaier, A., and Kennedy, A., 2000, Multistage Variscan magmatism in the central Tauern Window (Austria) unveiled by U/Pb SHRIMP zircon data: Contributions to Mineralogy and Petrology, v. 139, p. 418–435, https://doi.org/10.1007/s004100000145.

Fernández, F.J., and Llana-Fúnez, S., 2016, Localización de la deformación en la zona de falla de Valdoviño (NO Macizo Ibérico) asistida por fluidos carbonatados ricos en Fe y el crecimiento de filosilicatos: Geo-Temas, v. 16, no. 1, p. 41–44.

Fernández-Lozano, J., Pastor-Galán, D., Gutiérrez-Alonso, G., and Franco, P., 2016, New kinematic constraints on the Cantabrian orocline: A paleomagnetic study from the Peñalba and Truchas synclines, NW Spain: Tectonophysics, v. 681, p. 195–208, https://doi.org/10.1016/j.tecto.2016.02.019.

Fernández-Suárez, J., Gutiérrez-Alonso, G., Jenner, G.A., and Jackson, S.E., 1998, Geochronology and geochemistry of the Pola de Allande granitoids (northern Spain): Their bearing on the Cadomian–Avalonian evolution of northwest Iberia: Canadian Journal of Earth Sciences, v. 35, p. 1439–1453, https://doi.org/10.1139/e98-074.

Fernández-Suárez, J., Dunning, G.R., Jenner, G.A., and Gutiérrez-Alonso, G., 2000, Variscan collisional magmatism and deformation in NW Iberia: Constraints from U-Pb geochronology of granitoids: Journal of the Geological Society [London], v. 157, p. 565–576, https://doi.org/10.1144/jgs.157.3.565.

Fernández-Suárez, J., Gutiérrez-Alonso, G., Johnston, S.T., Jeffries, T.E., Pastor-Galán, D., Jenner, G.A., and Murphy, J.B., 2011, Iberian late-Variscan granitoids: Some considerations on crustal sources and the significance of "mantle extraction ages": Lithos, v. 123, p. 121–132, https://doi.org/10.1016/j.lithos.2010.09.010.

Fernández-Suárez, J., Gutiérrez-Alonso, G., Pastor-Galán, D., Hofmann, M., Murphy, J.B., and Linnemann, U., 2014, The Ediacaran–Early Cambrian detrital zircon record of NW Iberia: Possible sources and paleogeographic constraints: International Journal of Earth Sciences, v. 103, p. 1335–1357, https://doi.org/10.1007/s00531-013-0923-3.

Finger, F., Gerdes, A., Janousek, V., Rene, M., and Riegler, G., 2007, Resolving the Variscan evolution of the Moldanubian sector of the Bohemian Massif: The significance of the Bavarian and the Moravo-Moldanubian tectonometamorphic phases: Journal of Geosciences, v. 52, p. 9–28, 10.3190/jgeosci.005.

Finger, F., and Schiller, D., 2012, Lead contents of S-type granites and their petrogenetic significance: Contributions to Mineralogy and Petrology, v. 164, p. 747–755, https://doi.org/10.1007/s00410-012-0771-3.

Franco, M.P., and García de Figuerola, L.C., 1986, Las rocas básicas y ultrabásicas en el extremo occidental de la Sierra de Ávila: Studia Geologica Salmanticencia, v. 23, p. 193–219.

Franke, W., 1989, Tectonostratigraphic units in the Variscan belt of central Europe, *in* Dallmeyer, R.D., ed., Terranes in the Circum-Atlantic Paleozoic orogens: Geological Society of America Special Paper 230, p. 67–90, https://doi.org/10.1130/SPE230-p67.

Frei, D., and Gerdes, A., 2009, Precise and accurate in situ U-Pb dating of zircon with high sample throughput by automated LA-SF-ICP-MS: Chemical Geology, v. 261, p. 261–270, https://doi.org/10.1016/j.chemgeo.2008.07.025.

Frost, B.R., Barnes, C.G., Collins, W.J., Arculus, R.J., Ellis, D.J., and Frost, C.D., 2001, A geochemical classification for granitic rocks: Journal of Petrology, v. 42, p. 2033–2048, https://doi.org/10.1093/petrology/42.11.2033.

Galán, G., Pin, C., and Duthou, J.L., 1996, Sr-Nd isotopic record of multi-stage interactions between mantle-derived magmas and crustal components in a collision context—The ultramafic-granitoid association from Vivero (Hercynian belt, NW Spain): Chemical Geology, v. 131, p. 67–91, https://doi.org/10.1016/0009-2541(96)00027-7.

Galán, G., Corretgé, L.G., and Laurent, O., 1997, Low-potassium vaugnerites from Guéret (Massif Central, France). Mafic magma evolution influenced by contemporaneous granitoids: Mineralogy and Petrology, v. 59, p. 165–187, https://doi.org/10.1007/BF01161858.

Gallastegui, G., 2005, Petrología del macizo granodiorítico de Bayo-Vigo (Provincia de Pontevedra, España): Serie Nova Terra 26: Laboratorio Xeoloxico de Laxe. Área de Xeoloxía e Minería do Seminario de Estudos Galegos, 414 p.

GEODE, 2017, Mapa Geológico Digital continuo de España, scale 1:50,000: Instituto Geológico y Minero de España, http://mapas.igme.es/gis/rest/services/Cartografia_Geologica/IGME_Geode_50/MapServer/kml/mapl mage.kmz (accessed January 2017)

Gladney, E.R., Braid, J.A., Murphy, J.B., Quesada, C., and McFarlane, C.R., 2014, U-Pb geochronology and petrology of the late Paleozoic Gil Márquez pluton: Magmatism in the Variscan suture zone, southern Iberia, during continental collision and the amalgamation of Pangea: International Journal of Earth Sciences, v. 103, p. 1433–1451, https://doi.org/10.1007/s00531-014-1034-5.

Gloaguen, E., 2006, Apports d'une étude intégrée sur les relations entre granites et minéralisations filoniennes (Au et Sn-W) en contexte tardiorogénique (Chaîne Hercynienne, Galice centrale, Espagne) [Ph.D. thesis]: Orléans, France, Université d'Orléans, 575 p.

Gloaguen, E., Ruffet, G., Monié, P., Barbanson, L., Branquet, Y., Chauvet, A., and Bouchot, V., 2006, Geochronological constraints on the magmatic and hydrothermal evolution of the Tras-os-Montes Hercynian domain (Galica, Spain): Position of the Au, Sn-W mineralizing events, *in* Colloque Transmet, 2006, France: Société Française de Minéralogie et de Cristallographie, p. 111–114.

Gómez Barreiro, J., Wijbrans, J.R., Castiñeiras, P., Martínez Catalán, J.R., Arenas, R., Díaz García, F., and Abati, J., 2006, $^{40}Ar/^{39}Ar$ laserprobe dating of mylonitic fabrics in a polyorogenic terrane of NW Iberia: Journal of the Geological Society [London], v. 163, p. 61–73, https://doi.org/10.1144/0016-764905-012.

Gómez Barreiro, J., Martínez Catalán, J.R., Díez Fernández, R., Arenas, R., and Díaz García, F., 2010, Upper crust reworking during gravitational collapse: the Bembibre–Pico Sacro detachment system (NW Iberia): Journal of the Geological Society [London], v. 167, p. 769–784, https://doi.org/10.1144/0016-76492009-160.

González-Clavijo, E., Díez-Balda, M.A., and Álvarez Lobato, F., 1993, Structural study of a semiductile strike-slip system in the Central Iberian Zone (Variscan Fold Belt, Spain): Structural controls on gold deposits: Geologische Rundschau, v. 82, p. 448–460, https://doi.org/10.1007/BF00212409.

González Lodeiro, F., Hernández Urroz, J., Klein, E., Martínez Catalán, J.R., and De Pablo Maciá, J.G., 1984, Hoja y Memoria del Mapa Geológico Nacional, 1:200.000 n° 7 (Santiago de Compostela): Madrid, Instituto Geológico y Minero de España, 99 p.

Gutiérrez-Alonso, G., Fernández-Suárez, J., and Weil, A.B., 2004, Orocline triggered lithospheric delamination, *in* Sussman, A.J., and Weil, A.B., eds., Orogenic curvature: Integrating paleomagnetic and structural analyses: Geological Society of America Special Paper 383, p. 121–130, https://doi.org/10.1130/0-8137-2383-3(2004)383[121:OTLD]2.0.CO;2.

Gutiérrez-Alonso, G., Murphy, J.B., Fernández-Suárez, J., and Hamilton, M.A., 2008, Rifting along the northern Gondwana margin and the evolution of the Rheic Ocean: A Devonian age for the El Castillo volcanic rocks (Salamanca, Central Iberian Zone): Tectonophysics, v. 461, p. 157–165, https://doi.org/10.1016/j.tecto.2008.01.013.

Gutiérrez-Alonso, G., Fernández-Suárez, J., Jeffries, T.E., Johnston, S.T., Pastor-Galán, D., Murphy, J.B., Franco, M.P., and Gonzalo, J.C., 2011, Diachronous post-orogenic magmatism within a developing orocline in Iberia, European Variscides: Tectonics, v. 30, p. 1–17, https://doi.org/10.1029/2010TC002845.

Gutiérrez-Alonso, G., Collins, A.S., Fernández-Suárez, J., Pastor-Galán, D., González-Clavijo, E., Jourdan, F., Weil, A.B., and Johnston, S.T., 2015, Dating of lithospheric buckling: $^{40}Ar/^{39}Ar$ ages of syn-orocline strike-slip shear zones in northwestern Iberia: Tectonophysics, v. 643, p. 44–54, https://doi.org/10.1016/j.tecto.2014.12.009.

Hopkinson, T.N., Harris, N.B., Warren, C.J., Spencer, C.J., Roberts, N.M., Horstwood, M.S., and Parrish, R.R., 2017, The identification and significance of pure sediment-derived granites: Earth and Planetary Science Letters, v. 467, p. 57–63, https://doi.org/10.1016/j.epsl.2017.03.018.

Janoušek, V., and Holub, F.V., 2007, The causal link between HP-HT metamorphism and ultrapotassic magmatism in collisional orogens: Case study from the Moldanubian Zone of the Bohemian Massif: Proceedings of the Geologists' Association, v. 118, p. 75–86, https://doi.org/10.1016/S0016-7878(07)80049-6.

Jesus, A.P., Munhá, J., Mateus, A., Tassinari, C., and Nutman, A.P., 2007, The Beja layered gabbroic sequence (Ossa-Morena Zone, Southern Portugal): Geochronology and geodynamic implications: Geodinamica Acta, v. 20, p. 139–157, https://doi.org/10.3166/ga.20.139-157.

Julivert, M., 1971, Décollement tectonics in the Hercynian Cordillera of northwest Spain: American Journal of Science, v. 270, p. 1–29, https://doi.org/10.2475/ajs.270.1.1.

Klein, E., 1982, Mapa Geológico Nacional 1:50000 (MAGNA): Hoja y Memoria 153 (Cerdedo): Madrid, Instituto Geológico y Minero de España, 71 p.

Kroner, U., and Romer, R.L., 2013, Two plates—Many subduction zones: The Variscan orogeny reconsidered: Gondwana Research, v. 24, p. 298–329, https://doi.org/10.1016/j.gr.2013.03.001.

Kubínová, Š., Faryad, S.W., Verner, K., Schmitz, M., and Holub, F., 2017, Ultrapotassic dykes in the Moldanubian Zone and their significance for understanding of the post-collisional mantle dynamics during Variscan orogeny in the Bohemian Massif: Lithos, v. 272, p. 205–221, https://doi.org/10.1016/j.lithos.2016.12.007.

Laurent, O., Couzinié, S., Zeh, A., Vanderhaeghe, O., Moyen, J.F., Villaros, A., Gardien, V., and Chelle-Michou, C., 2017, Protracted, coeval crust and mantle melting during Variscan late-orogenic evolution: U-Pb dating in the eastern French Massif Central: International Journal of Earth Sciences, v. 106, p. 421–451, https://doi.org/10.1007/s00531-016-1434-9.

Ledru, P., Courrioux, G., Dallain, C., Lardeaux, J.-M., Montel, J.-M., Vanderhaeghe, O., and Vitel, G., 2001, The Velay dome (French Massif Central): Melt generation and granite emplacement during orogenic evolution: Tectonophysics, v. 342, p. 207–237, https://doi.org/10.1016/S0040-1951(01)00165-2.

Li, X.H., Faure, M., and Lin, W., 2014, From crustal anatexis to mantle melting in the Variscan orogen of Corsica (France): SIMS U-Pb zircon age constraints: Tectonophysics, v. 634, p. 19–30, https://doi.org/10.1016/j.tecto.2014.07.021.

Linnemann, U., Pereira, F., Jeffries, T.E., Drost, K., and Gerdes, A., 2008, The Cadomian Orogeny and the opening of the Rheic Ocean: The diacrony of geotectonic processes constrained by LA-ICP-MS U-Pb zircon dating (Ossa-Morena and Saxo-Thuringian Zones, Iberian and Bohemian Massifs): Tectonophysics, v. 461, p. 21–43, https://doi.org/10.1016/j.tecto.2008.05.002.

López-Carmona, A., Pitra, P., and Abati, J., 2013, Blueschist-facies metapelites from the Malpica-Tui Unit (NW Iberian Massif): Phase equilibria modelling and H_2O and Fe_2O_3 influence in high-pressure assemblages: Journal of Metamorphic Geology, v. 31, p. 263–280, https://doi.org/10.1111/jmg.12018.

López-Carmona, A., Abati, J., Pitra, P., and Lee, J.K.W., 2014, Retrogressed lawsonite blueschists from the NW Iberian Massif: *P–T–t* constraints from thermodynamic modelling and $^{40}Ar/^{39}Ar$ geochronology: Contributions to Mineralogy and Petrology, v. 167, p. 987, https://doi.org/10.1007/s00410-014-0987-5.

López-Moro, F.J., Moro, M.C., Timón, S.M., Cembranos, M.L., and Cózar, J., 2013, Constraints regarding gold deposition in episyenites: The Permian episyenites associated with the Villalcampo shear zone, central western Spain: International Journal of Earth Sciences, v. 102, p. 721–744, https://doi.org/10.1007/s00531-012-0844-6.

López-Moro, F.J., López-Plaza, M., Gutiérrez-Alonso, G., Fernández-Suárez, J., López-Carmona, A., Hofmann, M., and Romer, R.L., 2018, Crustal melting and recycling: Geochronology and sources of Variscan syn-kinematic anatectic granitoids of the Tormes Dome (Central Iberian Zone). A U-Pb LA-ICP-MS study: International Journal of Earth Sciences, p. 1–20, https://doi.org/10.1007/s00531-017-1483-8.

López Plaza, M., and Martínez Catalán, J.R., 1987, Síntesis estructural de los granitoides hercínicos del Macizo Hespérico, *in* Bea, F., et al., eds., Geología de los granitoides y rocas asociadas del Macizo Hesperico, libro homenaje a L. C. García de Figuerola: Madrid, Rueda, p. 195–210.

Lotze, F., 1945, Zur gliederung der variszíden der Iberischen Meseta: Geotektonische Forschungen, v. 6, p. 78–92.

Ludwig, K.R., 2012, User's manual for Isoplot/Ex, v. 3.75: A geochronological toolkit for Microsoft Excel: Berkeley Geochronology Center Special Publication 5, 75 p., http://www.bgc.org/isoplot_etc/isoplot/Isoplot3_75-4_15manual.pdf.

Marquínez, J., 1984, La geología del área esquistosa de Galicia Central (Cordillera Hercíniana, NW de España): Memorias del Instituto Geológico y Minero de España 100, 231 p.

Martín Garro, J., 2015, Geocronología de U/Pb mediante LA-ICP-MS en circones del Complejo anatéctico de Toledo y el batolito de los Montes de Toledo [M.S. thesis]: Salamanca, Spain, Salamanca University, 50 p.

Martínez Catalán, J.R., Arenas, R., Díaz García, F., Rubio Pascual, F.J., Abati, J., and Marquínez, J., 1996, Variscan exhumation of a subducted Paleozoic continental margin: The Basal Units of the Órdenes Complex, Galicia, NW Spain: Tectonics, v. 15, p. 106–121, https://doi.org/10.1029/95TC02617.

Martínez Catalán, J.R., Arenas, R., Díaz García, F., and Abati, J., 1997, Variscan accretionary complex of northwest Iberia: Terrane correlation and succession of tectonothermal events: Geology, v. 25, p. 1103–1106, https://doi.org/10.1130/0091-7613(1997)025<1103:VACONI>2.3.CO;2.

Martínez Catalán, J.R., Díaz García, F., Arenas, R., Abati, J., Castiñeiras, P., González Cuadra, P., Gómez Barreiro, J., and Rubio Pascual, F.J., 2002, Thrust and detachment systems in the Ordenes Complex (northwestern Spain): Implications for the Variscan-Appalachian geodynamics, *in* Martínez Catalán, J.R., et al., eds., Variscan-Appalachian dynamics: The building of the late Paleozoic basement: Geological Society of America Special Paper 364, p. 163–182, https://doi.org/10.1130/0-8137-2364-7.163.

Martínez Catalán, J.R., et al., 2007, Space and time in the tectonic evolution of the northwestern Iberian Massif: Implications for the Variscan belt, *in* Hatcher, R.D., Jr., et al., eds., 4-D framework of continental crust: Geological Society of America Memoir 200, p. 403–423, https://doi.org/10.1130/2007.1200(21).

Martínez Catalán, J.R., Rubio Pascual, F.J., Díez Montes, A., Díez Fernández, R., Gómez Barreiro, J., Dias da Silva, Í., González Clavijo, E., Ayarza, P., and Alcock, J.E., 2014, The late Variscan HT/LP metamorphic event in NW and Central Iberia: Relationships to crustal thickening, extension, orocline development and crustal evolution, *in* Schulmann, K., et al., eds., The Variscan orogeny: Extent, timescale and the formation of the European crust: Geological Society of London Special Publication 405, p. 225–247, https://doi.org/10.1144/SP405.1.

Martínez Catalán, J.R., González Clavijo, E., Meireles, C., Díez Fernández, R., and Bevis, J., 2016, Relationships between syn-orogenic sedimentation and nappe emplacement in the hinterland of the Variscan belt in NW Iberia deduced from detrital zircons: Geological Magazine, v. 153, p. 38–60, https://doi.org/10.1017/S001675681500028X.

Matte, P., 1986, Tectonics and plate tectonics model for the Variscan belt of Europe: Tectonophysics, v. 126, p. 329–374, https://doi.org/10.1016/0040-1951(86)90237-4.

Matte, P., 2001, The Variscan collage and orogeny (480-290 Ma) and the tectonic definition of the Armorica microplate: A review: Terra Nova, v. 13, p. 122–128, https://doi.org/10.1046/j.1365-3121.2001.00327.x.

Merino-Tomé, O., Gutiérrez-Alonso, G., Villa, E., Fernández-Suárez, J., Llaneza, J.M., and Hofmann, M., 2017, LA-ICP-MS U-Pb dating of Carboniferous ash layers in the Cantabrian Zone (N Spain): Stratigraphic implications: Journal of the Geological Society [London], v. 174, p. 836–849, https://doi.org/10.1144/jgs2016-119.

Mezger, J.E., and Gerdes, A., 2016, Early Variscan (Visean) granites in the core of central Pyrenean gneiss domes: Implications from laser ablation U-Pb and Th-Pb studies: Gondwana Research, v. 29, p. 181–198, https://doi.org/10.1016/j.gr.2014.11.010.

Miller, C.F., McDowell, S.M., and Mapes, R.W., 2003, Hot and cold granites? Implications of zircon saturation temperatures and preservation of inheritance: Geology, v. 31, p. 529–532, https://doi.org/10.1130/0091-7613(2003)031<0529:HACGIO>2.0.CO;2.

Montero, P., Salman, K., Bea, F., Azor, A., Expósito, I., González Lodeiro, F., Poyatos, D., and Simancas, F., 2000, New data on the geochronology of the Ossa-Morena Zone, Iberian Massif: Basement Tectonics, v. 15, p. 136–138.

Montero, P., Bea, F., González-Lodeiro, F., Talavera, C., and Whitehouse, M.J., 2007, Zircon ages of the metavolcanic rocks and metagranites of the Ollo de Sapo Domain in central Spain: Implications for the Neoproterozoic to early Palaeozoic evolution of Iberia: Geological Magazine, v. 144, p. 963–976, https://doi.org/10.1017/S0016756807003858.

Montero, P., Talavera, C., and Bea, F., 2017, Geochemical, isotopic, and zircon (U-Pb, O, Hf isotopes) evidence for the magmatic sources of the volcano-plutonic Ollo de Sapo Formation, Central Iberia: Geologica Acta, v. 15, p. 245–260, http://dx.doi.org/10.1344/%25x.

Monteserín, V., 1981. Mapa Geológico Nacional 1:50000 (MAGNA): Hoja y Memoria 186 (Puente Caldelas): Instituto Geológico y Minero de España, 33 p.

Moreno-Ventas, I., Rogers, G., and Castro, A., 1995, The role of hybridization in the genesis of Hercynian granitoids in the Gredos massif, Spain: Inferences from Sr-Nd isotopes: Contributions to Mineralogy and Petrology, v. 120, p. 137–149, https://doi.org/10.1007/BF00287111.

Moyen, J.F., Laurent, O., Chelle-Michou, C., Couzinié, S., Vanderhaeghe, O., Zeh, A., Villaros, A., and Gardien, V., 2017, Collision vs. subduction-related magmatism: Two contrasting ways of granite formation and implications for crustal growth: Lithos, v. 277, p. 154–177, https://doi.org/10.1016/j.lithos.2016.09.018.

Murphy, J.B., Gutiérrez-Alonso, G., Nance, R.D., Fernández-Suarez, J., Keppie, J.D., Quesada, C., Strachan, R.A., and Dostal, J., 2006, Origin of the Rheic Ocean: Rifting along a Neoproterozoic suture?: Geology, v. 34, p. 325–328, https://doi.org/10.1130/G22068.1.

Murphy, J.B., Gutiérrez-Alonso, G., Fernández-Suárez, J., and Braid, J.A., 2008, Probing crustal and mantle lithosphere origin through Ordovician volcanic rocks along the Iberian passive margin of Gondwana: Tectonophysics, v. 461, p. 166–180, https://doi.org/10.1016/j.tecto.2008.03.013.

Murphy, J.B., Nance, R.D., and Cawood, P.A., 2009, Contrasting modes of supercontinent formation and the conundrum of Pangea: Gondwana Research, v. 15, p. 408–420, https://doi.org/10.1016/j.gr.2008.09.005.

Nance, R.D., Gutiérrez-Alonso, G., Keppie, J.D., Linnemann, U., Murphy, J.B., Quesada, C., Strachan, R.A., and Woodcock, N.H., 2010, Evolution of the Rheic ocean: Gondwana Research, v. 17, p. 194–222, https://doi.org/10.1016/j.gr.2009.08.001.

Ordóñez Casado, B., 1998, Geochronological studies of the Pre-Mesozoic basement of the Iberian Massif: The Ossa Morena zone and the allochthonous complexes within the Central Iberian zone [Ph.D. thesis]: ETH Zurich, 235 p.

Ordóñez Casado, B., Martín-Izard, A., and García-Nieto, J., 2008, SHRIMP-zircon U-Pb dating of the Ni-Cu-PGE mineralized Aguablanca gabbro and Santa Olalla granodiorite: Confirmation of an Early Carboniferous metallogenic epoch in the Variscan Massif of the Iberian Peninsula: Ore Geology Reviews, v. 34, p. 343–353, https://doi.org/10.1016/j.oregeorev.2008.03.002.

Orejana, D., Villaseca, C., Pérez-Soba, C., López-García, J.A., and Billström, K., 2009, The Variscan gabbros from the Spanish Central System: A case for crustal recycling in the sub-continental lithospheric mantle?: Lithos, v. 110, p. 262–276, https://doi.org/10.1016/j.lithos.2009.01.003.

Orejana, D., Villaseca, C., Valverde-Vaquero, P., Belousova, E.A., and Armstrong, R.A., 2012, U-Pb geochronology and zircon composition of late Variscan S- and I-type granitoids from the Spanish Central System batholith: International Journal of Earth Sciences, v. 101, p. 1789–1815, https://doi.org/10.1007/s00531-012-0750-y.

Orejana, D., Losantos, E., Villaseca, C., and Jeffries, T.E., 2015, Mineral chemistry of late Variscan gabbros from central Spain: Constraints on crystallisation processes and nature of the parental magmas: Journal of Iberian Geology, v. 41, p. 253–272, https://doi.org/10.5209/rev_JIGE.2015.v41.n2.49178.

Ortega, L.A., 1998, Estudio petrogenético del granito sincinemático de dos micas de A Espenuca (A Coruña): Serie Nova Terra 14: Laboratorio Xeolóxico de Laxe Seminario de Estudos Galegos, Area de Xeoloxia e Mineria, 740 p.

Ortega, L.A., Carracedo, M., Larrea, F.J., and Gil Ibarguchi, J.I., 1994, Geoquímica del granito de dos micas de A Espenuca: Origen y evolución: Cadernos do Laboratorio Xeolóxico de Laxe, v. 19, p. 319–334.

Parga Pondal, I., 1956, Nota explicativa del mapa geológico de la parte NO de la provincia de La Coruña: Leidse Geologische Mededelingen, v. 21, p. 467–484.

Parga-Pondal, I., Vegas, R., and Marcos, A., 1982, Mapa Xeolóxico do Macizo Hespérico: Publicacions da Area de Xeoloxía e Minería do Seminario de Estudos Galegos, 14 p., scale 1:500,000.

Pastor-Galán, D., Gutiérrez-Alonso, G., Murphy, J.B., Fernández-Suárez, J., Hofmann, M., and Linnemann, U., 2013, Provenance analysis of the Paleozoic sequences of the northern Gondwana margin in NW Iberia: Passive margin to Variscan collision and orocline development: Gondwana Research, v. 23, p. 1089–1103, https://doi.org/10.1016/j.gr.2012.06.015.

Pastor-Galán, D., Ursem, B., Meere, P.A., and Langereis, C., 2015, Extending the Cantabrian orocline to two continents (from Gondwana to Laurussia): Paleomagnetism from south Ireland: Earth and Planetary Science Letters, v. 432, p. 223–231, https://doi.org/10.1016/j.epsl.2015.10.019.

Pastor-Galán, D., Dekkers, M.J., Gutiérrez-Alonso, G., Brouwer, D., Groenewegen, T., Krijgsman, W., Fernández-Lozano, J., Yenes, M., and Álvarez-Lobato, F., 2016, Paleomagnetism of the Central Iberian curve's putative hinge: Too many oroclines in the Iberian Variscides: Gondwana Research, v. 39, p. 96–113, https://doi.org/10.1016/j.gr.2016.06.016.

Pearce, J.A., Harris, N.B., and Tindle, A.G., 1984, Trace element discrimination diagrams for the tectonic interpretation of granitic rocks: Journal of Petrology, v. 25, p. 956–983, https://doi.org/10.1093/petrology/25.4.956.

Pereira, M.F., Chichorro, M., Williams, I.S., Silva, J.B., Fernández, C., Díaz-Azpiroz, M., Apraiz, A., and Castro, A., 2009, Variscan intra-orogenic extensional tectonics in the Ossa-Morena Zone (Évora-Aracena-Lora del Río metamorphic belt, SW Iberian Massif): SHRIMP zircon U-Th-Pb geochronology, *in* Murphy J.B., et al., eds., Ancient orogens and modern analogues: Geological Society of London Special Publication 327, p. 215–237, https://doi.org/10.1144/SP327.11.

Pereira, M.F., Chichorro, M., Moita, P., Santos, J.F., Solá, A.M.R., Williams, I.S., Silva, J.B., and Armstrong, R.A., 2015, The multistage crystallization of zircon in calc-alkaline granitoids: U-Pb age constraints on the timing of Variscan tectonic activity in SW Iberia: International Journal of Earth Sciences, v. 104, p. 1167–1183, https://doi.org/10.1007/s00531-015-1149-3.

Pereira, M.F., Díez Fernández, R., Gama, C., Hofmann, M., Gärtner, A., and Linnemann, U., 2018, S-type granite generation and emplacement during a regional switch from extensional to contractional deformation (Central Iberian Zone, Iberian autochthonous domain, Variscan Orogeny): International Journal of Earth Sciences, p. 1–17, https://doi.org/10.1007/s00531-017-1488-3 (in press).

Pin, C., Fonseca, P.E., Paquette, J.L., Castro, P., and Matte, P., 2008, The ca. 350 Ma Beja Igneous Complex: A record of transcurrent slab break-off in the Southern Iberia Variscan Belt?: Tectonophysics, v. 461, p. 356–377, https://doi.org/10.1016/j.tecto.2008.06.001.

Ribeiro, A., et al., 2007, Geodynamic evolution of the SW Europe Variscides: Tectonics, v. 26, TC6009, https://doi.org/10.1029/2006TC002058.

Ries, A.C., 1979, Variscan metamorphism and K-Ar dates in the Variscan fold belt of S Brittany and NW Spain: Journal of the Geological Society [London], v. 136, p. 89–103, https://doi.org/10.1144/gsjgs.136.1.0089.

Rodríguez-Alonso, M.D., Peinado, M., López-Plaza, M., Franco, P., Carnicero, A., and Gonzalo, J.C., 2004, Neoproterozoic–Cambian synsedimentary magmatism in the Central Iberian Zone (Spain): Geology, petrology and geodynamic significance: International Journal of Earth Sciences, v. 93, p. 897–920, https://doi.org/10.1007/s00531-004-0425-4.

Rodríguez, J., Cosca, M.A., Gil Ibarguchi, J.I., and Dallmeyer, R.D., 2003, Strain partitioning and preservation of $^{40}Ar/^{39}Ar$ ages during Variscan exhumation of a subducted crust (Malpica-Tui complex, NW Spain): Lithos, v. 70, p. 111–139, https://doi.org/10.1016/S0024-4937(03)00095-1.

Rodríguez, J., Gil Ibarguchi, J.I., and Paquette, J., 2007, Sincronía del magmatismo varisco en el Macizo Ibérico: nuevas edades U-Pb en granitoides de la región de Finisterre (La Coruña, España): XV Semana-VI Congreso Ibérico de Geoquímica, p. 146–149 (DVD-ROM).

Rodríguez Fernández, L.R., et al., 2004, Mapa tectónico de España con la inclusión de Portugal continental y Pirineos Franceses, *in* Vera, J.A., ed., Geología de España: Geological Society of Spain, Instituto Geológico y Minero de España, 884 p.

Romeo, I., Lunar, R., Capote, R., Quesada, C., Dunning, G.R., Piña, R., and Ortega, L., 2006, U-Pb age constraints on Variscan magmatism and Ni-Cu-PGE metallogeny in the Ossa-Morena Zone (SW Iberia): Journal of the Geological Society [London], v. 163, p. 837–846, https://doi.org/10.1144/0016-76492005-065.

Rossi, P., Oggiano, G., and Cocherie, A., 2009, A restored section of the "southern Variscan realm" across the Corsica-Sardinia microcontinent: Comptes Rendus Geoscience, v. 341, p. 224–238, https://doi.org/10.1016/j.crte.2008.12.005.

Rubio-Ordóñez, A., Gutiérrez-Alonso, G., Valverde-Vaquero, P., Cuesta, A., Gallastegui, G., Gerdes, A., and Cárdenes, V., 2015, Arc-related Ediacaran magmatism along the northern margin of Gondwana: Geochronology and isotopic geochemistry from northern Iberia: Gondwana Research, v. 27, p. 216–227, https://doi.org/10.1016/j.gr.2013.09.016.

Rubio Pascual, F.J., Arenas, R., Martínez Catalán, J.R., Rodríguez Fernández, L.R., and Wijbrans, J.R., 2013, Thickening and exhumation of the Variscan roots in the Iberian Central System: Tectonothermal processes and $^{40}Ar/^{39}Ar$ ages: Tectonophysics, v. 587, p. 207–221, https://doi.org/10.1016/j.tecto.2012.10.005.

Santos Zalduegui, J.F., 1995, Geocronología y geoquímica isotópica de diferentes unidades de los complejos alóctonos de Cabo Ortegal y Malpica-Tuy (NO de España): Serie Nova Terra 11: A Coruña, Spain, Laboratorio Xeolóxico de Laxe, 178 p.

Scarrow, J.H., Molina, J.F., Bea, F., and Montero, P., 2009, Within-plate calc-alkaline rocks: Insights from alkaline mafic magma–peraluminous crustal melt hybrid appinites of the Central Iberian Variscan continental collision: Lithos, v. 110, p. 50–64, https://doi.org/10.1016/j.lithos.2008.12.007.

Schaltegger, U., 1997, Magma pulses in the Central Variscan Belt: Episodic melt generation and emplacement during lithospheric thinning: Terra Nova, v. 9, p. 242–245, https://doi.org/10.1111/j.1365-3121.1997.tb00021.x.

Schaltegger, U., 2000, U-Pb geochronology of the Southern Black Forest Batholith (Central Variscan Belt): Timing of exhumation and granite emplacement: International Journal of Earth Sciences, v. 88, p. 814–828, https://doi.org/10.1007/s005310050308.

Schulmann, K., Schaltegger, U., Jezek, J., Thompson, A.B., and Edel, J.B., 2002, Rapid burial and exhumation during orogeny: Thickening and synconvergent exhumation of thermally weakened and thinned crust (Variscan orogen in western Europe): American Journal of Science, v. 302, p. 856–879, https://doi.org/10.2475/ajs.302.10.856.

Schulmann, K., Lexa, O., Janoušek, V., Lardeaux, J.M., and Edel, J.B., 2014, Anatomy of a diffuse cryptic suture zone: An example from the Bohemian Massif, European Variscides: Geology, v. 42, p. 275–278, https://doi.org/10.1130/G35290.1.

Serrano Pinto, M., Casquet, C., Ibarrola, E., Corretgé, G., and Portugal Ferreira, M., 1987, Síntese geocronológica dos granitóides do Macizo Hespérico, *in* Bea, F., et al., eds., Geología de los granitoides y rocas asociadas del Macizo Hespérico, libro homenaje a L. C. García de Figuerola: Madrid, Rueda. p. 69–86.

Shand, S.J., 1943, Eruptive rocks: Their genesis, composition, and classification, with a chapter on meteorites: London, Thomas Murby and Co., 350 p.

Stacey, J.T., and Kramers, J.D., 1975, Approximation of terrestrial lead isotope evolution by a two-stage model: Earth and Planetary Science Letters, v. 26, p. 207–221, https://doi.org/10.1016/0012-821X(75)90088-6.

Sun, S.S., and McDonough, W.S., 1989, Chemical and isotopic systematics of oceanic basalts: Implications for mantle composition and processes, *in* Saunders, A.D., and Norry, M.J., eds., Magmatism in the ocean basins: Geological Society of London Special Publication 42, p. 313–345, https://doi.org/10.1144/GSL.SP.1989.042.01.19.

Tabaud, A.S., Janoušek, V., Skrzypek, E., Schulmann, K., Rossi, P., Whitechurch, H., Guerrot, C., and Paquette, J.L., 2015, Chronology, petrogenesis and heat sources for successive Carboniferous magmatic events in the Southern–Central Variscan Vosges Mts (NE France): Journal of the Geological Society [London], v. 172, p. 87–102, https://doi.org/10.1144/jgs2013-123.

Talavera, C., Montero, P., Bea, F., Lodeiro, F.G., and Whitehouse, M., 2013, U-Pb zircon geochronology of the Cambro-Ordovician metagranites and metavolcanic rocks of central and NW Iberia: International Journal of Earth Sciences, v. 102, p. 1–23, https://doi.org/10.1007/s00531-012-0788-x.

Teixeira, R.J.S., Neiva, A.M., Gomes, M.E.P., Corfu, F., Cuesta, A., and Croudace, I.W., 2012, The role of fractional crystallization in the genesis of early syn-D 3, tin-mineralized Variscan two-mica granites from the Carrazeda de Ansiães area, northern Portugal: Lithos, v. 153, p. 177–191, https://doi.org/10.1016/j.lithos.2012.04.024.

Ugidos, J.M., and Recio, C., 1993, Origin of cordierite-bearing granites by assimilation in the Central Iberian Massif (CIM), Spain: Chemical Geology, v. 103, p. 27–43, https://doi.org/10.1016/0009-2541(93)90289-U.

Valle Aguado, B., Azevedo, M.R., Schaltegger, U., Martínez Catalán, J.R., and Nolan, J., 2005, U-Pb zircon and monazite geochronology of Variscan magmatism related to syn-convergence extension in Central Northern Portugal: Lithos, v. 82, p. 169–184, https://doi.org/10.1016/j.lithos.2004.12.012.

Valverde-Vaquero, P., and Dunning, G.R., 2000, New U-Pb ages for Early Ordovician magmatism in central Spain: Journal of the Geological Society [London], v. 157, p. 15–26, https://doi.org/10.1144/jgs.157.1.15.

Vermeesch, P., 2012, On the visualisation of detrital age distributions: Chemical Geology, v. 312, p. 190–194, https://doi.org/10.1016/j.chemgeo.2012.04.021.

Villaseca, C., Barbero, L., and Rogers, G., 1998, Crustal origin of Hercynian peraluminous granitic batholiths of central Spain: Petrological, geochemical and isotopic (Sr, Nd) arguments: Lithos, v. 43, p. 55–79, https://doi.org/10.1016/S0024-4937(98)00002-4.

Villaseca, C., Downes, H., Pin, C., and Barbero, L., 1999, Nature and composition of the lower continental crust in central Spain and the granulite-granite linkage: Inferences from granulitic xenoliths: Journal of Petrology, v. 40, p. 1465–1496, https://doi.org/10.1093/petroj/40.10.1465.

Villaseca, C., Bellido, F., Pérez-Soba, C., and Billström, K., 2009, Multiple crustal sources for post-tectonic I-type granites in the Hercynian Iberian belt: Mineralogy and Petrology, v. 96, p. 197–211, https://doi.org/10.1007/s00710-009-0057-2.

Villaseca, C., Orejana, D., Belousova, E.A., Armstrong, R.A., Pérez-Soba, C., and Jeffries, T.E., 2011, U-Pb isotopic ages and Hf isotope composition of zircons in Variscan gabbros from central Spain: Evidence of variable crustal contamination: Mineralogy and Petrology, v. 101, p. 151–167, https://doi.org/10.1007/s00710-010-0142-6.

von Raumer, J.F., Finger, F., Veselá, P., and Stampfli, G.M., 2014, Durbachites-vaugnerites—A geodynamic marker in the central European Variscan orogen: Terra Nova, v. 26, p. 85–95, https://doi.org/10.1111/ter.12071.

Watson, E.B., and Harrison, T.M., 1983, Zircon saturation revisited: Temperature and composition effects in a variety of crustal magma types: Earth and Planetary Science Letters, v. 64, p. 295–304, https://doi.org/10.1016/0012-821X(83)90211-X.

Weil, A.B., Gutiérrez-Alonso, G., Johnston, S.T., and Pastor-Galán, D., 2013, Kinematic constraints on buckling a lithospheric-scale orocline along the northern margin of Gondwana: A geologic synthesis: Tectonophysics, v. 582, p. 25–49, https://doi.org/10.1016/j.tecto.2012.10.006.

Žák, J., Sláma, J., and Burjak, M., 2017, Rapid extensional unroofing of a granite-migmatite dome with relics of high-pressure rocks, the Podolsko complex, Bohemian Massif: Geological Magazine, v. 154, p. 354–380, https://doi.org/10.1017/S0016756816000030.

MANUSCRIPT RECEIVED 27 SEPTEMBER 2017
REVISED MANUSCRIPT RECEIVED 22 NOVEMBER 2017
MANUSCRIPT ACCEPTED 24 JANUARY 2018